Electronic ISSN: 1309-0267

I J E A S

International Journal of Engineering & Applied Sciences

IJEAS

Volume 10, Issue 4
2018

Published by Akdeniz University

Editorial Board

(The name listed below is not Alphabetical or any title scale)

Abstracting & Indexing

IJEAS provides unique **DOI** link to every paper published.

Editorial Scope

The journal presents its readers with broad coverage across some branches of engineering and science of the latest development and application of new solution algorithms, artificial intelligent techniques innovative numerical methods and/or solution techniques directed at the utilization of computational methods in solid and nano-scaled mechanics.

International Journal of Engineering & Applied Sciences (IJEAS) is an Open Access Journal

International Journal of Engineering & Applied Sciences (IJEAS) publish original contributions on the following topics:

Numerical Methods in Solid Mechanics

Nanomechanic and applications

Microelectromechanical systems (MEMS)

Vibration Problems in Engineering

Higher order elasticity (Strain gradient, couple stress, surface elasticity, nonlocal elasticity)

Applied Mathematics

CONTENTS

International Journal of Engineering & Applied Sciences (IJEAS)
Vol.10, Issue 4 (2018)276-290
http://dx.doi.org/10.24107/ijeas.481462
Int J Eng Appl Sci 10(4) (2018) 276-290

The Complementary Functions Method Solution to the Functionally Graded Polar Orthotropic Rotating Hyperbolic Disks with Both Radially and Circumferentially Aligned Fibers

Vebil Yıldırım

Department of Mechanical Engineering, Faculty of Engineering, University of Çukurova, Adana
E-mail address: vebil@cu.edu.tr

ORCID numbers of authors:
0000-0001-9955-8423

Received date: 11.11.2018
Accepted date: 07.12.2018

Abstract

In the present study, efforts have been made to numerically evaluate elastic displacements and stresses in a convergent or divergent hyperbolic disk subjected to a centrifugal force of constant circular velocity. The disk material is assumed to be continuously radially functionally graded (FG) with two orthotropic materials based on the simplest Voigt rule with a power of volume fraction of two constituents. The fibers are assumed to be aligned along either radial (RR) or circumferential (CR) directions. Having been a second order differential equation with variable coefficients, the governing equation so-called Navier equation is first derived and then put in the form of two differential equations of first order. These two ordinary differential equation set is originally solved based on the initial value problem (IVP) by employing the Complementary Functions Method (CFM). The numerical results are verified with the corresponding benchmark results for uniform thickness FG polar orthotropic disks. The radial variation of the elastic fields in a hyperbolic disk is investigated for several boundary conditions, disk profile parameters, and the gradient parameter for both the radially and circumferentially aligned fibers. Some numerical results are also presented. Under the case that is considered in this study, it is revealed that the CR disk offers much higher elastic fields than RR disk under all boundary conditions. For a composite rotating disk rotating at a constant speed, it will be better to align fibers along the radial directions, to use convergent disk profiles, and to locate the material having higher radial stiffness at the outer surface. It is also disclosed that the location of the maximum Von-Mises equivalent stress in fixed-free disks varies regarding the fiber orientation.

Keywords: Anisotropic, complementary functions method, composite rotating disk, elasticity solution, functionally graded, initial value problem, polar orthotropic, variable-thickness, Voigt rule.

1. Introduction

Rotating disks are essential elements of turbine rotors, compressors, flywheels, automobile disc brake systems, gears, and etc. Today's scientific works focus on the use of advanced materials so that discs can withstand much higher rotational speeds and resulting stresses.

Rotating disk is a common component in diverse engineering applications such as turbine rotors, compressors, flywheels, disk brakes in automobiles, gears, computer disk drives, and etc.

Anisotropic materials whose mechanical properties change in certain directions allow engineers to design and manufacture rotating disks that can withstand much higher critical/burst speeds than those made from common isotropic materials. As a new kind of advanced structural composite materials, FGMs have made considerable headway since the 1990s by virtue of their impeccable heat-resistance features. Despite the open literature contains many studies having very high academic standard on anisotropic disks, on FG metal-ceramic disks or the disks which are functionally graded with isotropic materials, any of them is not included in this article due to the space limitation.

Using anisotropic/orthotropic materials to form FG new kind nonhomogeneous materials is also one of the new trends in engineering design. There are, therefore, a limited number of works on FG disks composed of anisotropic materials in the open literature [1-8]. From those, Durodola and Attia [1] considered FG orthotropic materials to study deformation and stresses in rotating hollow uniform disks. Chen et al. [2] offered a three-dimensional analytical solution for a uniform rotating disk made of exponentially functionally graded materials with transverse isotropy. Kansal and Parvez [3] dealt with stress analysis on orthotropic graded rotating annular disks subjected to parabolic temperature distributions. Lubarda [4] analytically and numerically studied the elastic response of a uniformly pressurized cylindrically anisotropic hollow uniform thin rotating disks by using both the finite difference method and a Fredholm integral equation. Fredholm integral equation was also employed by Peng and Li [5] to consider FG hollow polar-orthotropic rotating disks under free-free and fixed-free boundary conditions. Kacar and Yıldırım [6] offered analytical formulas for the displacement and stress determination in polar orthotropic functionally power-law graded polar orthotropic rotating uniform disks under three boundary conditions. Essa and Argeso [7] developed analytical solutions for the analysis of elastic polar orthotropic FG annular free-free and fixed-free disks rotating with constant angular velocity. The elasticity moduli and thickness were assumed to be varied radially by a nonlinear function controlled by three parameters, while the radial variation of density may be defined by any form of continuous function. Essa and Argeso [7] also validated their analytical solutions by the use of a computational model based on the nonlinear shooting method. Based on the finite difference method and Voigt grading rule, Zheng et al. [8] numerically studied displacements and stress fields in a functionally graded fiber reinforced non-uniform thickness disk mounted on a rotating shaft and subjected to angular deceleration. The disk profile in the form of $(\alpha / r + \beta)$ and circumferentially reinforced fibers were considered in this comprehensive study. Zheng et al. [8] concluded that the disk deceleration has no effect on the radial and hoop stresses except the shear stress.

As seen from the open literature that there are few studies considered the CR-disks (Fig. 1) [8-12]. As far as the author knows, moreover, there is scarcely any comparative study on the elastic behavior of functionally graded CR and RR orthotropic disks. This was also a motivation for the author.

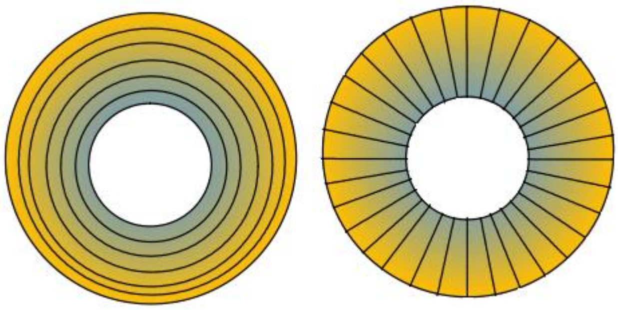

CR-disk RR-disk

Fig. 1. Circumferentially and radially aligned disks

In this work, a comprehensive analysis that inspects the elastic characteristics of both RR and CR disks made of FG orthotropic materials and having either divergent or convergent hyperbolic disk profiles is presented (Figs. 1-2). A Voigt rule with a power of volume fraction of two orthotropic constituents is used to determine the radial variation of elastic constants. Poisson's ratios are taken to be constant. Within the frame of infinitesimal deformations and axisymmetric plane stress elasticity theory, Navier equation is derived and solved numerically based on the Complementary Functions Method (CFM) under three types of boundary conditions: free-free (traction-free inner and outer surfaces), fixed-free (rigidly circular shaft-mounted inner surface and traction-free outer surface), and fixed-guided (rigidly circular shaft-mounted inner surface and rigidly-cased outer surface). The present results are verified with the available literature [5].

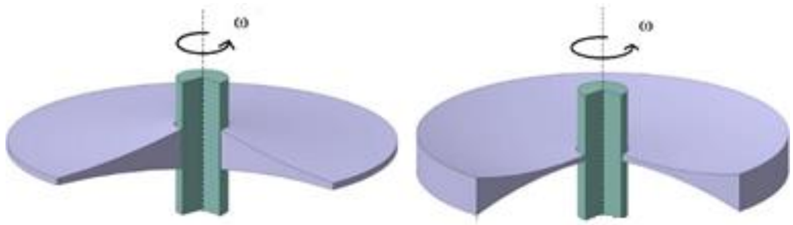

Convergent (m<0) Divergent (m>0)

Fig. 2. Convergent and divergent hyperbolic disk profiles

2. Derivation and Solution of Navier Equation

Under small deformation assumptions, the strain-displacement relation is given by

$$\varepsilon_r(r) = \frac{\mathrm{d}u_r(r)}{r}, \quad \varepsilon_\theta(r) = \frac{u_r(r)}{r} \tag{1}$$

By presuming a state of axisymmetric plane stress (since the thickness/diameter ratio is far less than one) constitutive equation for RR-disk is to be (for CR disk, simply use $E_1 = E_\theta, E_2 = E_r, \nu_{12=}\nu_{\theta r})$

$$\sigma_{\mathrm{r}}(\mathrm{r}) = -\frac{E_\theta \nu_{r\theta}}{\nu_{\theta r}(\nu_{r\theta}\nu_{\theta r}-1)}\varepsilon_r(r) - \frac{E_\theta \nu_{r\theta}}{(\nu_{r\theta}\nu_{\theta r}-1)}\varepsilon_\theta(\mathrm{r}) = C_{11}(r)\varepsilon_r(r) + C_{12}(r)\varepsilon_\theta(r) \tag{2}$$

$$\sigma_\theta(r) = -\frac{E_\theta \nu_{r\theta}}{(\nu_{r\theta}\nu_{\theta r}-1)}\varepsilon_r(r) - \frac{E_\theta}{(\nu_{r\theta}\nu_{\theta r}-1)}\varepsilon_\theta(r) = C_{12}(r)\varepsilon_r(r) + C_{22}(r)\varepsilon_\theta(r)$$

The equilibrium equation under the centrifugal forces is

$$\big(h(r)r\sigma_r(r)\big)' - h(r)\sigma_\theta(r) + \rho(r)h(r)\omega^2 r^2 = 0 \tag{3}$$

Poisson's ratio are related by Maxwell's theorem as follows

$$\frac{\nu_{\theta r}}{E_\theta(r)} = \frac{\nu_{r\theta}}{E_r(r)} \tag{4}$$

Navier equation is derived from the field equations given above as follows

$$\frac{d^2u_r(r)}{dr} + \left(\frac{1}{r} + \frac{\frac{dC_{11}(r)}{dr}}{C_{11}(r)} + \frac{\frac{dh(r)}{dr}}{h(r)}\right)\frac{du_r(r)}{dr} + \left(-\frac{C_{22}(r)}{r^2C_{11}(r)} + \frac{C_{12}(r)}{rC_{11}(r)}\left(\frac{\frac{dC_{11}(r)}{dr}}{C_{11}(r)} + \frac{\frac{dh(r)}{dr}}{h(r)}\right)\right)u_r(\mathrm{r}) = -\frac{\rho(r)\omega^2 r}{C_{11}(r)} \tag{5}$$

This equation is a second order differential equation with variable coefficients for boundary value problems (BVP). IVP form of the above Navier equation may be derived as follows

$$\frac{du_r(r)}{dr} = -\frac{E_\theta(r)\nu_{r\theta}}{rE_r(r)}u_r(r) - \frac{(\nu_{r\theta}\nu_{\theta r}-1)}{E_r(r)}\sigma_r(r) \tag{6a}$$

$$\frac{d\sigma_r(r)}{dr} = -\frac{E_\theta(r)\big(E_r(r) - E_\theta(r)\nu_{r\theta}^2\big)}{r^2E_r(r)(\nu_{r\theta}\nu_{\theta r}-1)}u_r(r) + \left(\frac{E_\theta(r)\nu_{r\theta}}{rE_r(r)} - \frac{1}{r} - \frac{\frac{dh(r)}{dr}}{h(r)}\right)\sigma_r(r) - \rho(r)\omega^2 r \tag{6b}$$

Equation (6) is written in a compact form of

$$\frac{d\boldsymbol{Z}(r)}{dr} = \boldsymbol{D}(r)\boldsymbol{Z}(r) + \boldsymbol{f}(r) \tag{7}$$

where

$$\boldsymbol{Z}(r) = \begin{Bmatrix} u_r(r) \\ \sigma_r(r) \end{Bmatrix} = \begin{Bmatrix} z_1(r) \\ z_2(r) \end{Bmatrix} \tag{8a}$$

$$\boldsymbol{f}(r) = \begin{Bmatrix} 0 \\ -\rho(r)\omega^2 r \end{Bmatrix} \tag{8b}$$

$$D_{11} = -\frac{E_\theta(r)\nu_{r\theta}}{rE_r(r)} \tag{8c}$$

$$D_{12} = -\frac{(\nu_{r\theta}\nu_{\theta r} - 1)}{E_r(r)} \tag{8d}$$

$$D_{21} = -\frac{E_\theta(r)\left(E_r(r) - E_\theta(r)\nu_{r\theta}^2\right)}{r^2E_r(r)(\nu_{r\theta}\nu_{\theta r} - 1)} \tag{8e}$$

$$D_{22} = \frac{E_\theta(r)\nu_{r\theta}}{rE_r(r)} - \frac{1}{r} - \frac{\frac{dh(r)}{dr}}{h(r)} \tag{8f}$$

The general solution of Eq. (7) in CFM over the interval [a, b] is given by [13-17]

$$\begin{aligned} z_1(r) &= x_0(r) + b_1x_1(r) + b_2x_2(r) \\ z_2(r) &= y_0(r) + b_1y_1(r) + b_2y_2(r) \end{aligned} \tag{9}$$

where unknown functions $x_{0,}\, x_1, x_2$ and $y_{0,}\, y_1, y_2$ are calculated by using those prescribed boundary conditions given in Table 1 in the first three stages of the method. At the final stage, the physical boundary conditions given in Table 2 are imposed in Eq. (9) to determine the remaining unknowns, b_1 and b_2. The solution has then been completed.

Table 1. Procedure for the first three steps of CFM

Let	Solve Eq.(7)	with the following prescribed initial conditions	Find
$\begin{Bmatrix} z_1 = x_0 \\ z_2 = y_0 \end{Bmatrix}$	with f(r)≠0	$\begin{Bmatrix} z_1(\text{a}) = 0 \\ z_2(\text{a}) = 0 \end{Bmatrix}$	$\begin{Bmatrix} x_0 \\ y_0 \end{Bmatrix}$
$\begin{Bmatrix} z_1 = x_1 \\ z_2 = y_1 \end{Bmatrix}$	with f(r)=0	$\begin{Bmatrix} z_1(\text{a}) = 1 \\ z_2(\text{a}) = 0 \end{Bmatrix}$	$\begin{Bmatrix} x_1 \\ y_1 \end{Bmatrix}$
$\begin{Bmatrix} z_1 = x_2 \\ z_2 = y_2 \end{Bmatrix}$	with f(r)=0	$\begin{Bmatrix} z_1(\text{a}) = 0 \\ z_2(\text{a}) = 1 \end{Bmatrix}$	$\begin{Bmatrix} x_2 \\ y_2 \end{Bmatrix}$

Table 2. Boundary conditions taken into consideration

	$r = \mathrm{a}$	$r = b$
Free-Free	$\sigma_r(a) = 0$	$\sigma_r(b) = 0$
Fixed-Free	$u_r(\mathrm{a}) = 0$	$\sigma_r(\mathrm{b}) = 0$
Fixed-Guided	$u_r(\mathrm{a}) = 0$	$u_r(\mathrm{b}) = 0$

3. Material and Geometry of the Disk

A hyperbolic disk profile function is determined as follows

$$h(r) = h_b \left(\frac{r}{b}\right)^m \tag{10}$$

In Eq. (10), m=0 represents the uniform disk. Positive profile parameters offer divergent hyperbolic disks while the negative ones render convergent disks (Fig. 2).

In the present study, Voigt rule is employed with a power of volume fraction of constituents as follows [5]

$$V_B = \left(\frac{r^n - a^n}{b^n - a^n}\right), n > 0 \tag{11}$$

In this function (Fig. 3), the outer surface is to be Material B-rich (woven Glass fiber/Epoxy prepreg) while the inner surface is Materal A-rich (An injection molded Nylon 6 composite containing 40 wt% short glass fiber) (Table 3).

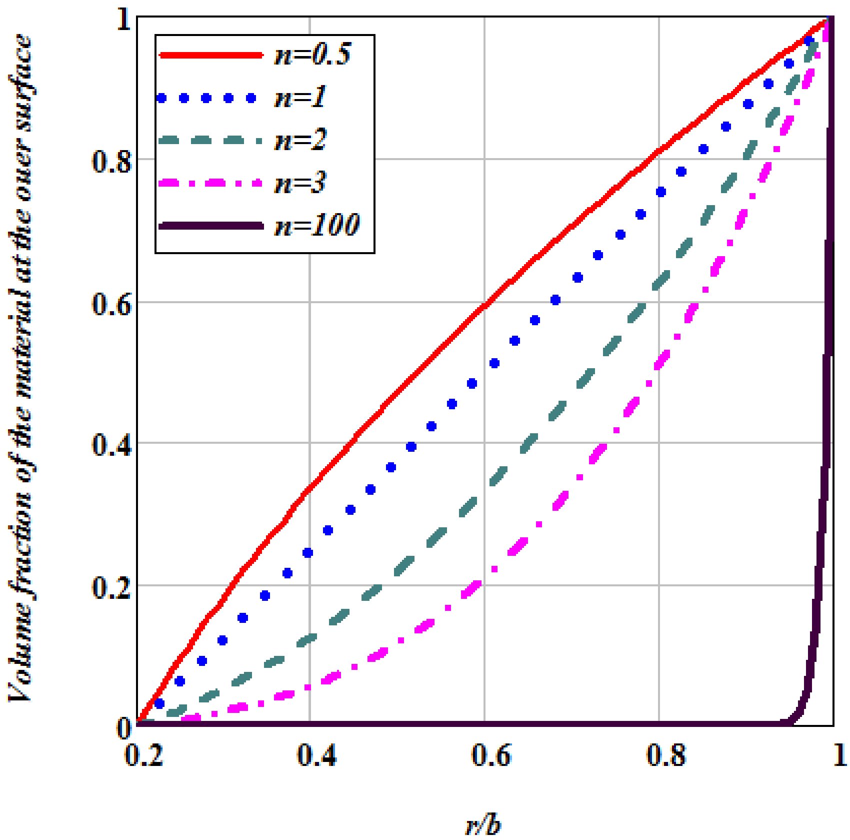

Fig. 3. Variation of volume fraction of the outer surface material

Table 3. Anisotropic materials and their properties.

	E_r (GPa)	E_θ(GPa)	ρ (kg/m^3)	$\nu_{r\theta}$
Material-A [18]	12.0	20.0	1600	0.21
Material-B [9]	21.8	26.95	2030	0.15

Based on the Voigt mixture rule, the radial variation of the effective material properties such as $E_r(r), E_\theta(r),$ and $\rho(r)$ are defined by

$$P(r) = P_A V_A + P_B V_B = P_A(1 - V_B) + P_B V_B = (P_B - P_A)V_B + P_A \tag{12}$$

It is worth noting that, in the present numerical analysis, the arithmetic mean of Poisson's ratios of two orthotropic materials is considered.

$$\nu_{r\theta} = \frac{\nu_{r\theta}^A + \nu_{r\theta}^B}{2} = constant \tag{13}$$

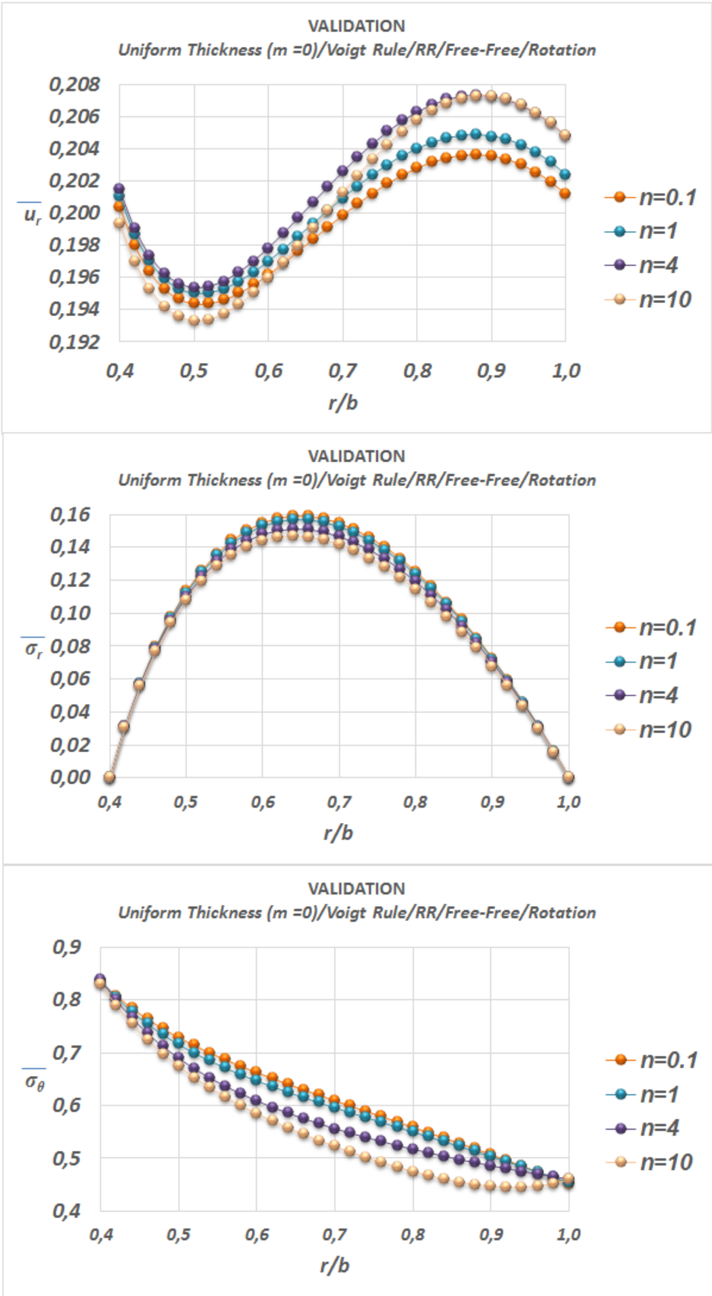

Fig. 4. Validation of the present results with Reference [5] ($\sigma_o = 12GPa.\rho_o = 1600kg/m^3$)

4. Numerical Study

The dimensionless elastic fields are defined as

$$\bar{u}_r = \frac{E_o}{\rho_o \omega^2 b^3} u_r, \bar{\sigma}_r = \frac{\sigma_r}{\rho_o \omega^2 b^2}, \bar{\sigma}_\theta = \frac{\sigma_\theta}{\rho_o \omega^2 b^2} \quad (14)$$

To verify the present numerical results with material properties given in Table 3, the example in Reference [5] is re-considered. Results are illustrated in Fig. 4.

Comparison of the graphs in Fig. 4 and Reference [5] shows a good harmony although very minor differences are observed in the variation of the radial displacement. The reason of this that Peng and Li [5] used $\nu_{r\theta} = 0.35 = constant$ along the radial coordinate. As stated before, the arithmetic mean of Poisson's ratios is employed in the present study as in Eq. (13).

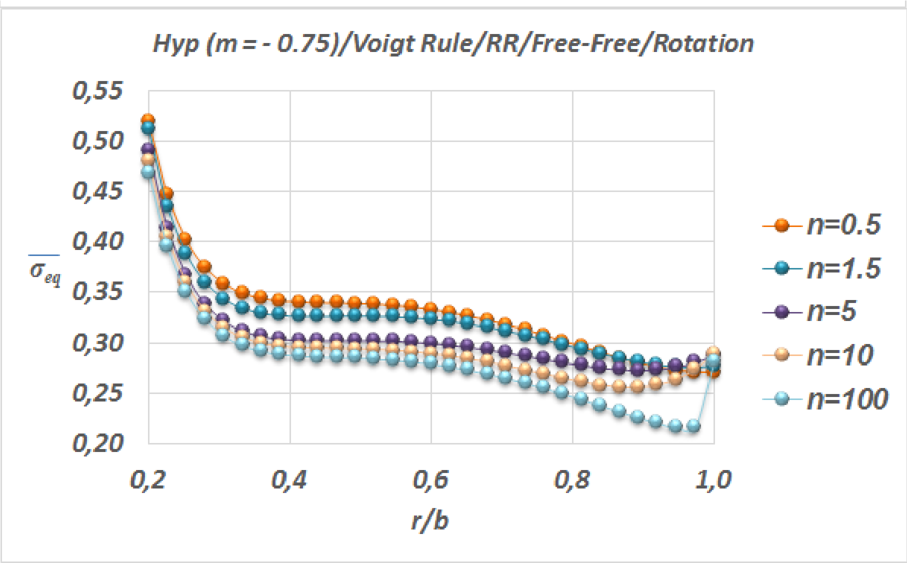

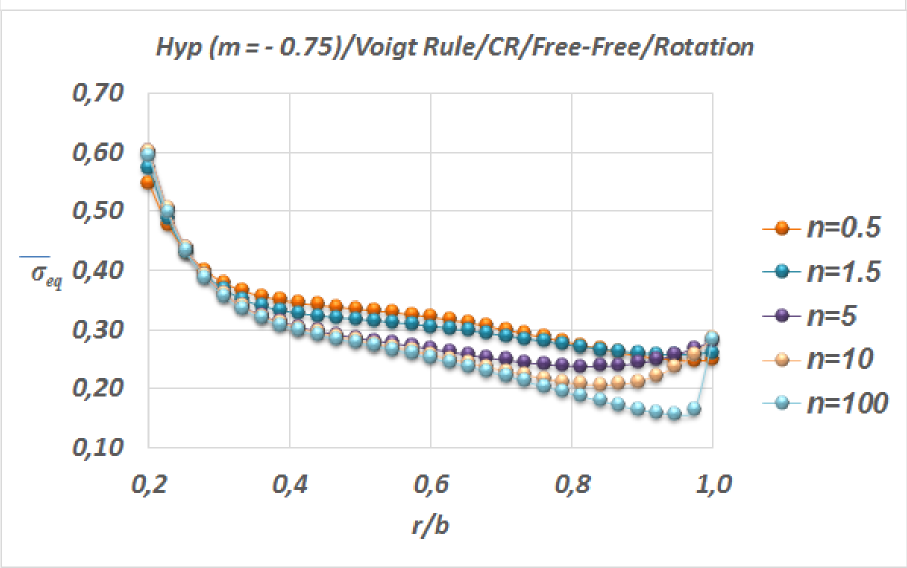

Fig. 5. Equivalent stress variation in a convergent free-free disk

Unless otherwise stated, $\sigma_o = 20GPa, \rho_o = 1600kg/m^3$, a/b=0.2 and material properties in Table 3 are used in the other examples in this section. The following is also to be used for calculation of the equivalent von-Mises stresses.

$$\sigma_{eq} = \sqrt{{\sigma_r}^2 - \sigma_r\sigma_\theta + {\sigma_\theta}^2} \tag{15}$$

Table 3. Elastic fields in a disk mounted a rigid shaft at its center for both RR-aligned and CR-aligned fibers (Fixed-Free / n=1.5/$\sigma_o = 20GPa, \rho_o = 1600kg/m^3$)

r/b	$\bar{u}_r$	$\bar{\sigma}_r$	$\bar{\sigma}_\theta$	$\bar{\sigma}_{eq}$
	m = - 0.75 (Convergent) - RR			
0.20	0.000000	0.254942	0.070393	0.228045
0.36	0.058276	0.267503	0.239232	0.254547
0.52	0.109178	0.267832	0.298127	0.284193
0.68	0.149197	0.226587	0.310756	0.278384
0.84	0.173387	0.138394	0.289906	0.251152
1.00	0.178150	0.000000	0.240057	0.240057
	m = - 0.75 (Convergent) - CR			
0.20	0.000000	0.397176	0.069018	0.367560
0.36	0.053761	0.367496	0.167605	0.318670
0.52	0.097730	0.329748	0.206547	0.288594
0.68	0.130795	0.260380	0.218750	0.242262
0.84	0.150247	0.152298	0.206644	0.185539
1.00	0.153441	0.000000	0.167250	0.167250
	m = 0 (Uniform) - RR			
0.20	0.000000	0.498896	0.137752	0.446261
0.36	0.093347	0.367826	0.367436	0.367631
0.52	0.155521	0.311798	0.407678	0.369197
0.68	0.197666	0.238967	0.397688	0.346737
0.84	0.220296	0.136596	0.359863	0.314649
1.00	0.223040	0.000000	0.300546	0.300546
	m = 0 (Uniform) - CR			
0.20	0.000000	0.857362	0.148986	0.793430
0.36	0.094259	0.542222	0.275015	0.469595
0.52	0.151229	0.400530	0.298017	0.360380
0.68	0.186970	0.281421	0.293677	0.287745
0.84	0.204963	0.152405	0.269602	0.234145
1.00	0.205853	0.000000	0.224380	0.224380
	m = 0.75 (Divergent) - RR			
0.20	0.000000	0.951731	0.262785	0.851320
0.36	0.145635	0.483175	0.549678	0.519628
0.52	0.217426	0.347049	0.548290	0.480397
0.68	0.258985	0.242830	0.504968	0.437422
0.84	0.278433	0.131066	0.445852	0.396896
1.00	0.278505	0.000000	0.375286	0.375286
	m = 0.75 (Divergent) - CR			
0.20	0.000000	1.809360	0.314418	1.674440
0.36	0.162007	0.767196	0.442271	0.666997
0.52	0.231863	0.464214	0.427418	0.446954
0.68	0.267464	0.291406	0.396815	0.356013
0.84	0.281906	0.147241	0.356954	0.310705
1.00	0.279353	0.000000	0.304494	0.304494

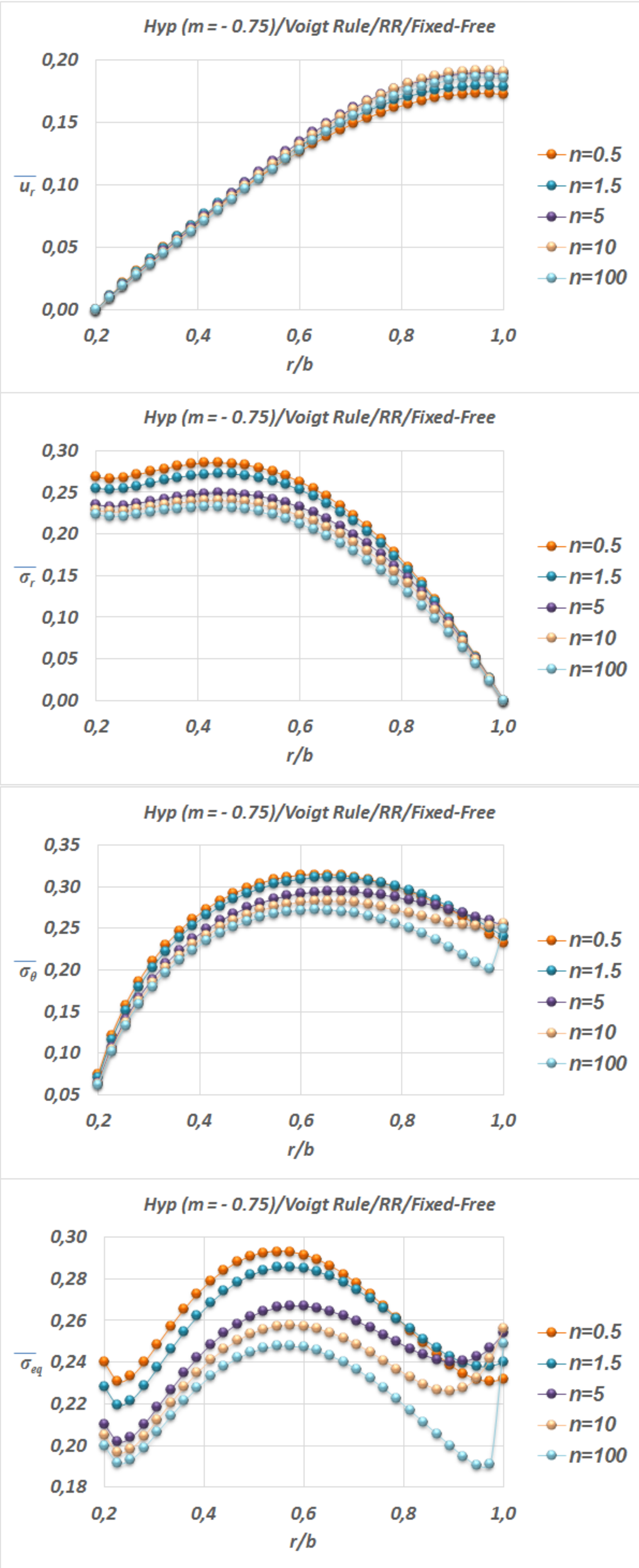

Fig. 6. Elastic fields in a convergent fixed-free RR-disk

Results are presented in Table 3 and Figs. 5-9 for various cases. As explained before, Young's modulus in the radial direction of the outer surface material (Material-B) is assumed to be higher than the other. Table 3 reveals that the convergent hyperbolic profile and RR orientation are better than uniform and divergent ones since they offer smaller equivalent stresses under rotation and fixed-free boundary conditions. Figs. 5-9 suggest that RR disks have smaller equivalent stresses than CR ones under all boundary conditions. Fig. 6 and 8 disclosed that the location of the maximum equivalent stress in fixed-free disk depends on the fiber orientation.

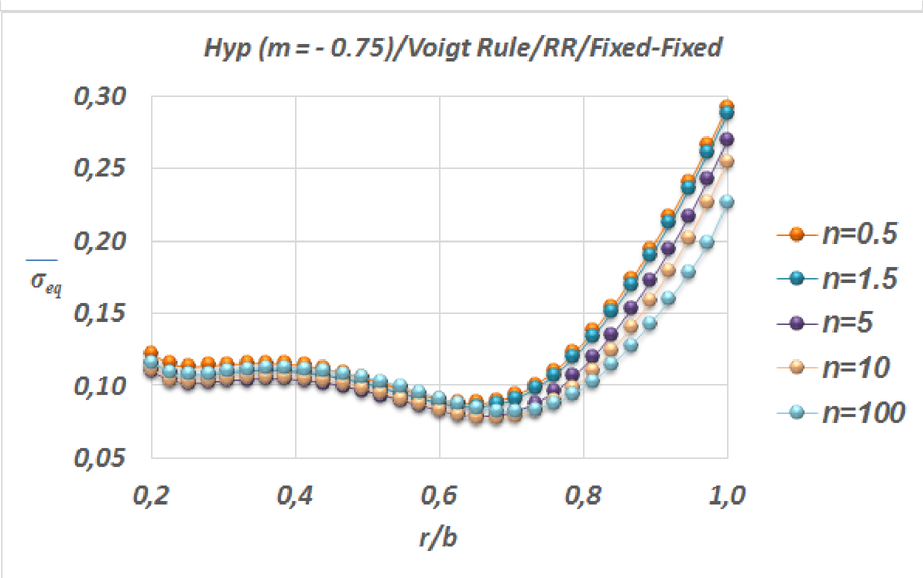

Fig. 7. Equivalent stress variation in a convergent fixed-fixed RR-disk

5. Conclusions

From the present study conducted with CFM the following results are achieved: i) CR-disks have higher equivalent stresses than RR-disks, ii) the location of the maximum Von-Mises equivalent stress in fixed-free disks depends on the fiber orientation, iii) if the outer surface material has higher radial stiffness than the inner surface material, a RR-disk having convergent profile has the smallest equivalent stresses than uniform and divergent ones under all boundary conditions.

Nomenclature

a, b : Inner and outer radii of the disk
C_{ij} : Stiffness components
$E(r)$: Effective Young's modulus
E_r, E_θ : Young's moduli along radial and tangential directions
$h(r)$: Disk profile function
m : Hyperbolic disk profile parameter
n : Gradation parameter
r, θ : Radial and tangential coordinates
u_r : Radial displacement
V : Volume fraction

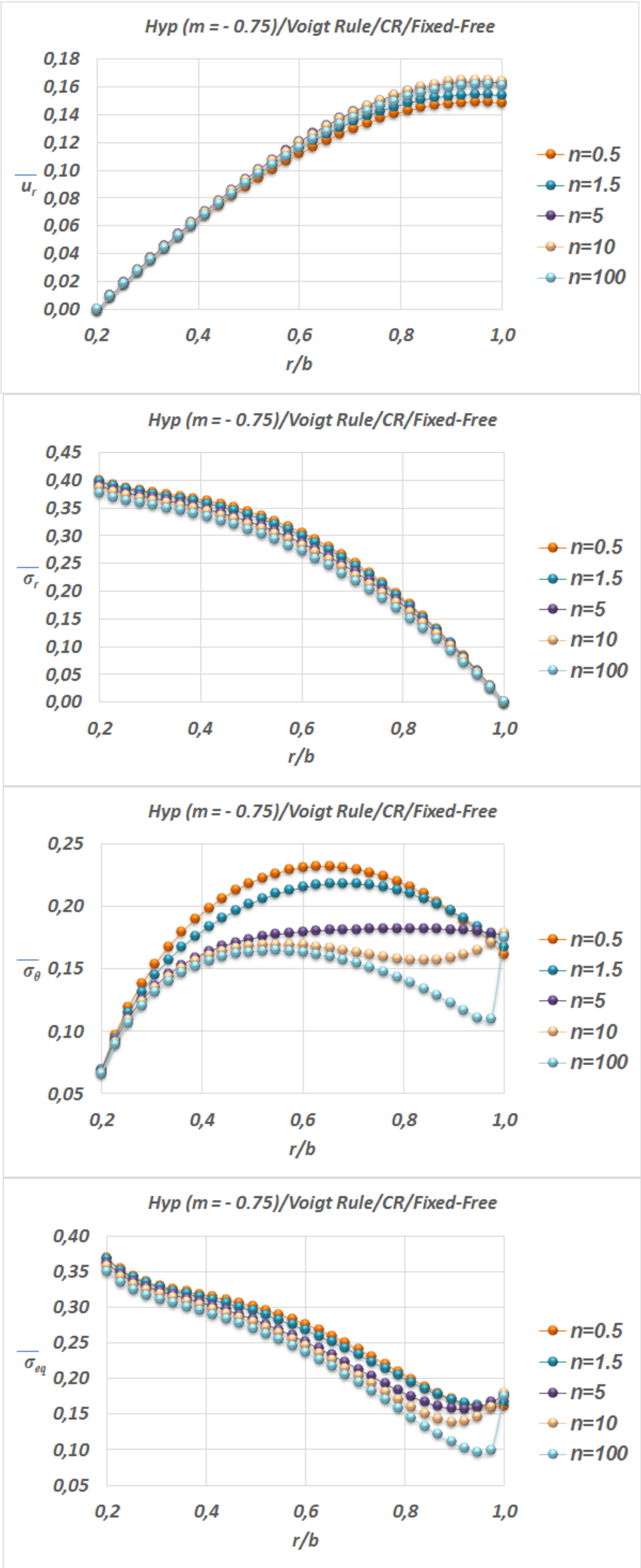

Fig. 8. Elastic fields in a convergent fixed-free CR-disk

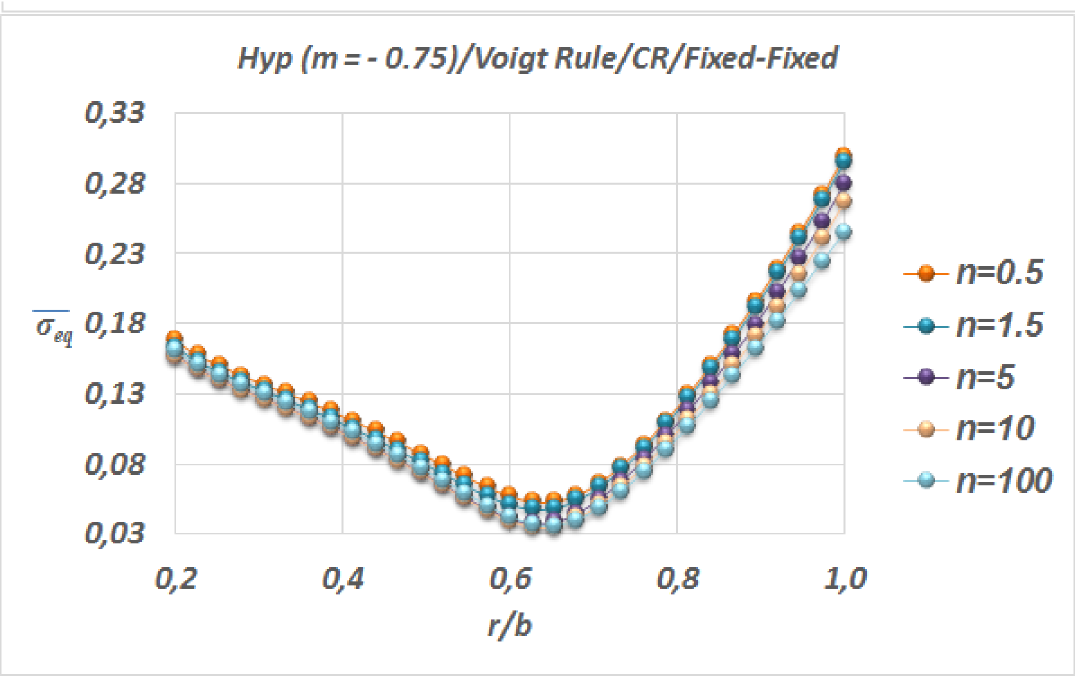

Fig. 9. Equivalent stress variation in a convergent fixed-fixed CR-disk

$\varepsilon_r, \varepsilon_\theta$: Radial and tangential normal strain components
ρ : Material density
σ_{eq} : Equivalent Von-Mises stress
σ_r, σ_θ : Normal radial and hoop stresses
ω : Circular frequency
$\nu_{r\theta}$, $\nu_{\theta r}$: Anisotropic Poisson's ratios

Subcripts

a, A : At the inner surface
b, B : At the outer surface
o : Reference value of the quantity

Overscripts

_ : Dimensionless quantity

References

[1] Durodola, J., Attia, O., Deformation and stresses in functionally graded rotating discs", Compos Sci Technol, 60, 987-995, 2000.

[2] Chen, J., Ding, H., Chen, W., Three-dimensional analytical solution for a rotating disc of functionally graded materials with transverse isotropy, Archive of Applied Mechanics, 77, 241-251, 2007.

[3] Kansal, G., Parvez, M., Thermal stress analysis of orthotropic graded rotating discs, International Journal of Modern Engineering Research (IJMER), 2(5), 3881-3885, 2012.

[4] Lubarda, V. A., On pressurized curvilinearly orthotropic circular disc, cylinder and sphere made of radially nonuniform material, Journal of Elasticity, 109, 103-133, 2012.

[5] Peng, X. L., Li, X. F., Elastic analysis of rotating functionally graded polar orthotropic discs, Int J Mech Sci, 60, 84-91, 2012.

[6] Kacar, I., Yıldırım, V., Effect of the anisotropy ratios on the exact elastic behavior of functionally power-graded polar orthotropic rotating uniform discs under various boundary conditions, Digital Proceeding of ICOCEE – Cappadocia 2017, Nevsehir, Turkey, 1743-1752, 2017.
[7] Essa, S., Argeso, H., Elastic analysis of variable profile and polar orthotropic FGM rotating disks for a variation function with three parameters, Acta Mech, 228, 3877–3899, 2017.
[8] Zheng, Y., Bahaloo, H., Mousanezhad, D., Vaziri, A., Nayeb-Hashemi, H., Displacement and stress fields in a functionally graded fiber-reinforced rotating disk with nonuniform thickness and variable angular velocity, J Eng Mater Technol, ASME, 39, 031010-1-9, 2017.
[9] Callioglu, H., Thermal stress analysis of curvilinearly orthotropic rotating discs, J Thermoplast Compos Mater, 20, 357-369, 2007.
[10] Callioglu, H., Topcu, M., Altan, G., Stress analysis of curvilinearly orthotropic rotating discs under mechanical and thermal loading, J Reinf Plast Compos, 24, 831-838, 2005.
[11] Tahani, M., Nosier, A., Zebarjad, S. M., Deformation and stress analysis of circumferentially fiber-reinforced composite disks, Int. J. Solids Struct, 42(9–10), 2741–2754, 2005.
[12] Zenkour A.M.,Allam N.M.N., On the rotating fiber-reinforced viscoelastic composite solid and annular disks of variable thickness, Int. J. Comput. Methods Eng. Sci Mech., 7, 21-31, 2006.
[13] Aktas, Z., Numerical Solutions of Two-Point Boundary Value Problems. Ankara, Turkey, METU, 1972.
[14] Roberts, S., Shipman, J., Fundamental matrix and two-point boundary-value problems, Journal of Optimization Theory and Applications, 28(1), 77-88, 1979.
[15] Haktanır, V., The complementary functions method for the element stiffness matrix of arbitrary spatial bars of helicoidal axes, Int J Numer Meth Eng, 38(6), 1031–1056, 1995.
[16] Yıldırım, V., Free vibration analysis of non-cylindrical coil springs by combined use of the transfer matrix and the complementary functions methods, Comm Numer Meth Eng, 13(6), 487–94, 1997.
[17] Yıldırım, V., The complementary functions method (CFM) solution to the elastic analysis of polar orthotropic rotating discs, J. Appl. Comput. Mech, 4(3), 216-230, 2018. DOI: 10.22055/JACM.2017.23188.1150
[18] Callioglu, H., Stress analysis of an orthotropic rotating disc under thermal loading, J Reinf Plast Compos, 23(17), 1857–1869, 2004.

International Journal of Engineering & Applied Sciences (IJEAS)
Vol.10, Issue 4 (2018)291-304
http://dx.doi.org/10.24107/ijeas.528290
Int J Eng Appl Sci 10(4) (2018) 291-304

Modal Analysis of Micro and Nanowires Using Finite Element Softwares

Kadir Mercan [a], Ömer Civalek [b]*

Department of Civil Engineering, Faculty of Engineering, Akdeniz University, Antalya, TURKIYE
**E-mail address: civalek@yahoo.com*

ORCID numbers of authors:
0000-0003-3657-6274[a], 0000-0003-1907-9479[b]

Received date: 23.12.2018
Accepted date: 15.02.2019

Abstract

The aim of this work is to represent a quick and truthful modality to obtain frequencies of microwires and nanowires which are widely used in nanosensors, nanocircuit and many more susceptible scientific areas. In this paper, modal analysis of micro and nano sized wires is investigated using COMSOL software. To obtain first ten mode shapes and eigenfrequencies of silicon carbide nanowire, thirty-nine modes is calculated. Results are given in figures captured from the software.

Keywords: Modal analysis, microwires, nanowires, SiCNW, COMSOL.

1. Introduction

As experimental analyzes of very small structures like carbon nanotubes (CNT), silicon carbide nanotubes (SiCNT), boron nitride nanotubes (BNNT), zinc oxide nanotube (ZnO) and nanowires of homologous structures is very-high costed and take a long time, many methods have been developed to make analysis possible without any experiment. Similarly, atomic simulation and molecular dynamic analysis need too much time to analyze nanotubes in case of buckling and vibration. Continuum mechanics models have been widely used to perform modal, dynamic and stability analysis using mathematical model [1-4]. Computer softwares have also been widely used to perform modal, dynamic and stability analysis in recent years [5-8]. Most of analysis softwares is not able to model structures in micro and nano size. Determining the critical buckling loads and frequencies of nanotubes is very important in case of designing for its particular using areas.

Finite element method (FEM) is a very time-effective method if meshing phase is done properly. This method has been used for a very wide range of analysis. Many different geometries can be modeled using the method such as very complex parts of engineering systems [9-15], beams, plates [16], shells [17, 18], human body parts such as kidney, bone etc. [19-22]. The computer software used to obtain mode shapes and eigenfrequencies is a finite element method based software.

2. Modelling Structures

Meshing is the most important part of software analyzes [23]. Inaccurate meshing leads to inaccurate results in modal, dynamic, and stability analyzes. For example, coarse meshing as it can be seen In Fig. 1 (a) would end up with improper results for current model. On the other hand, too fine meshing (Fig. 1 (c)) would end up with accurate and close results to experiments however analyzes would take very long time due to very much calculating vertexes in body.

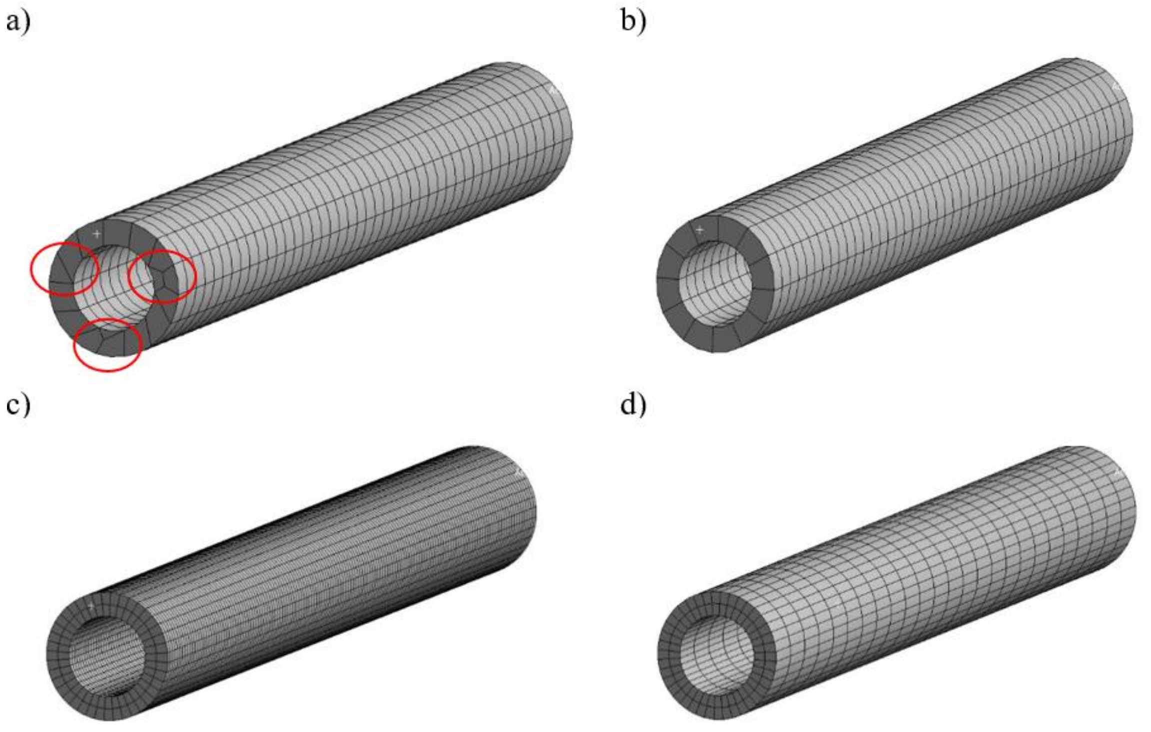

Fig. 1. Meshing nanostructures

Ideal meshing steps of a modeled nanotube is demonstrated in Fig. 1. respectively. In first step, skewed and irregular links between vertexes is observed and demonstrated in red circles (Fig. 1(a)). After fixing this issue (Fig. 1. (b)) it is observed that none of vertex were placed throughout the thickness of nanotube, this issue would lead to inaccurate results due to none of calculation throughout the thickness of nanotube. To overcome this issue, the spacing between vertexes is reduced (Fig. 1 (c)). As it can be seen in Fig. 1 (c). As it is stated before, too fine meshing would take very long time of analyzes due to very much calculating vertexes in body. Spacing between vertexes is extended for the body while reduced spacing is preserved along the thickness of nanostructure (Fig. 1 (d)).

3. Modal Analysis of SiCNW

COMSOL Multiphysics [24] is used to model and perform modal analysis on selected silicon carbide nanowire (SiCNW). Subsequent to meshing, needed material properties (Young's modulus 0.62 TPa and Poisson ratio 0.37) and geometrical properties is defined [25, 26]. Eventually, intended boundary conditions is defined (simply support in this case).

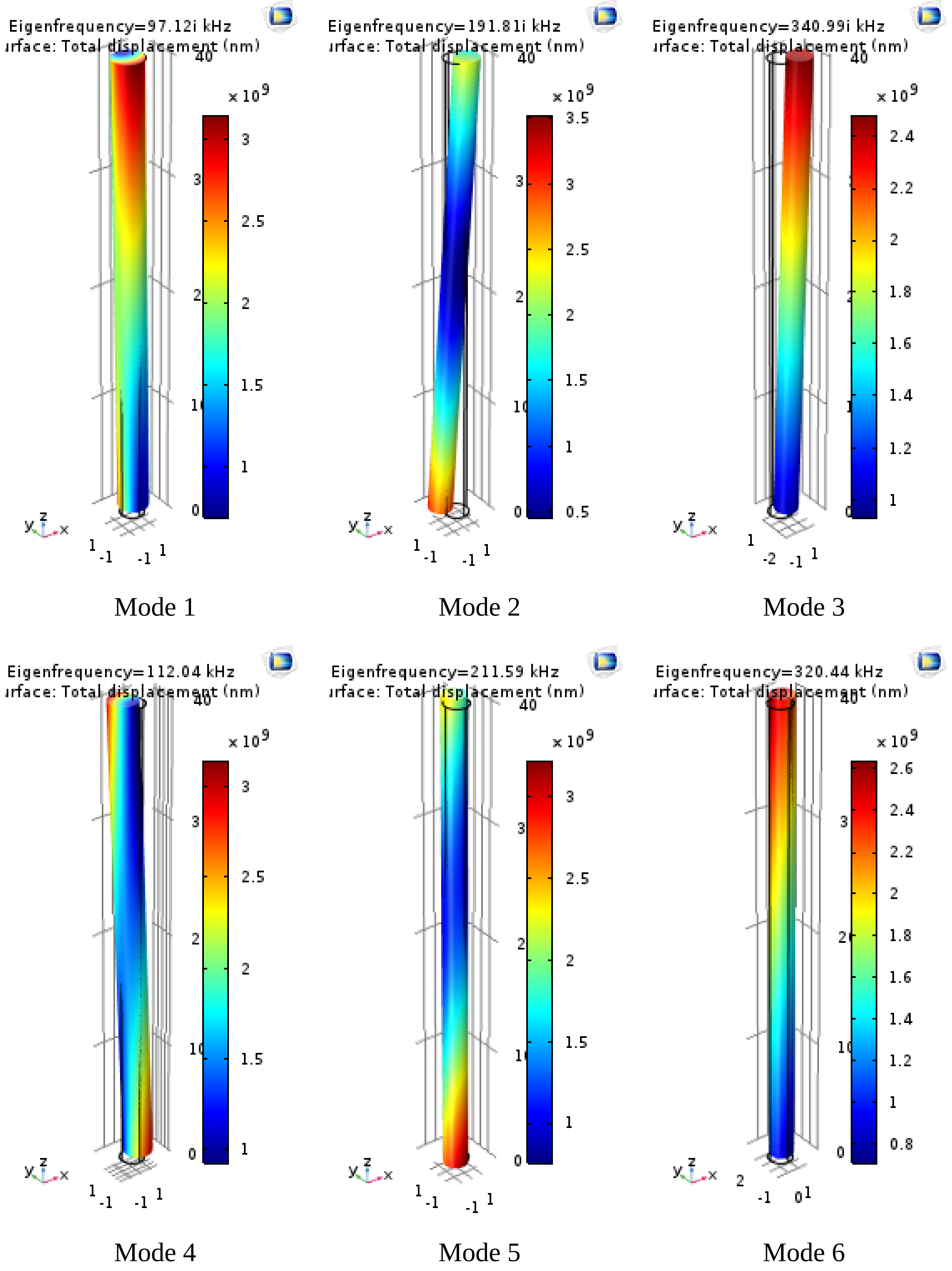

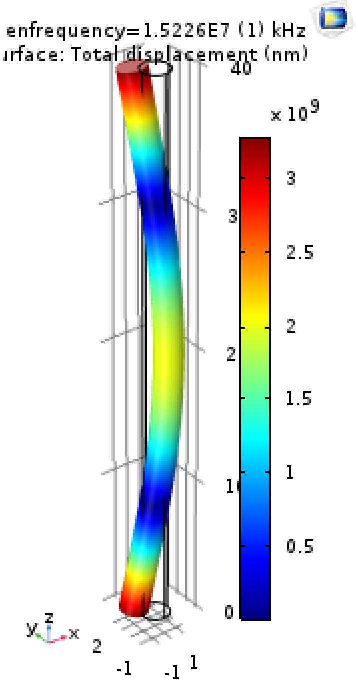

Mode 7

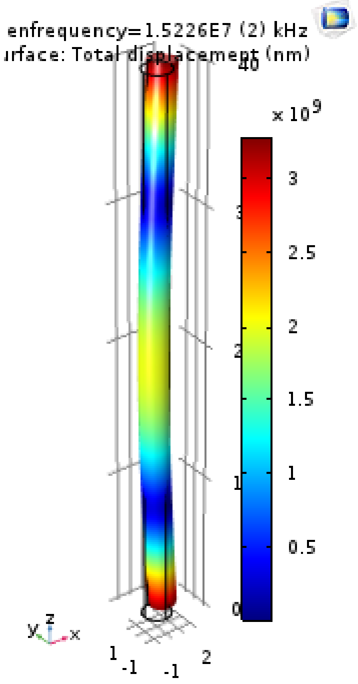

Mode 8

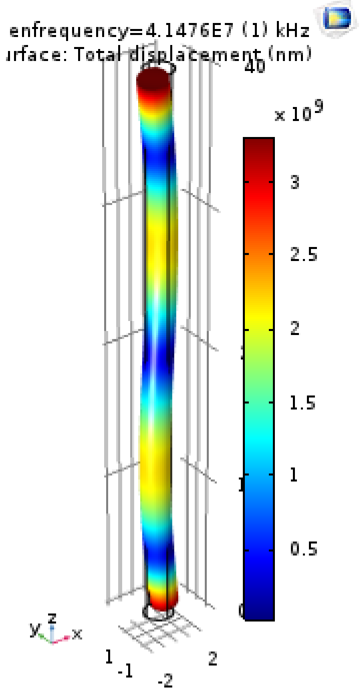

Mode 9

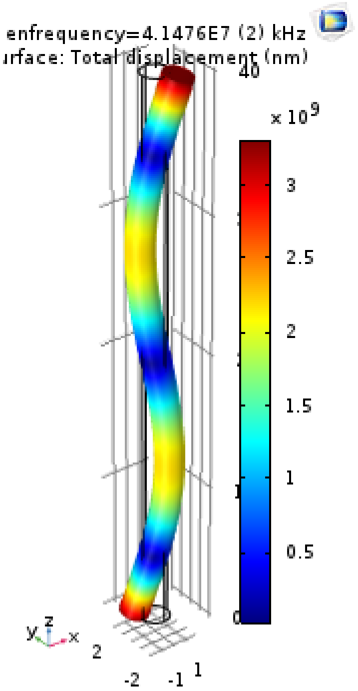

Mode 10

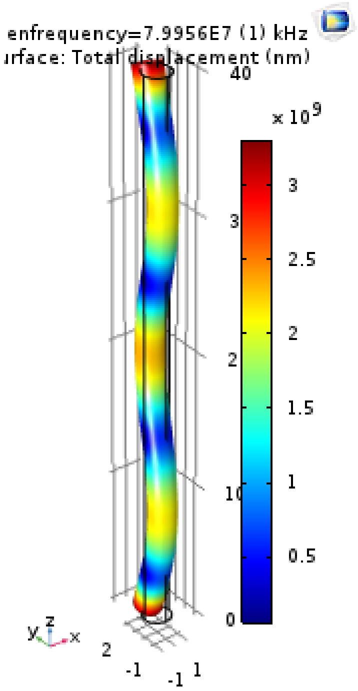

Mode 11

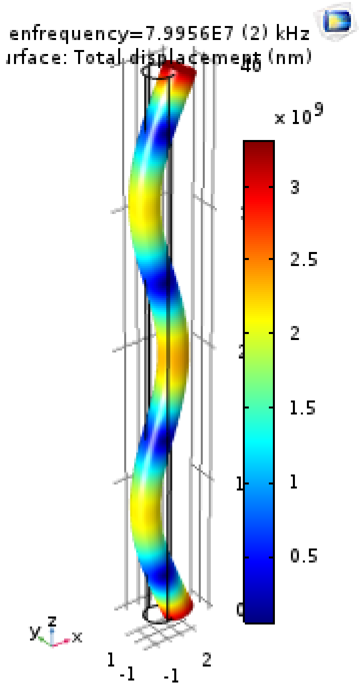

Mode 12

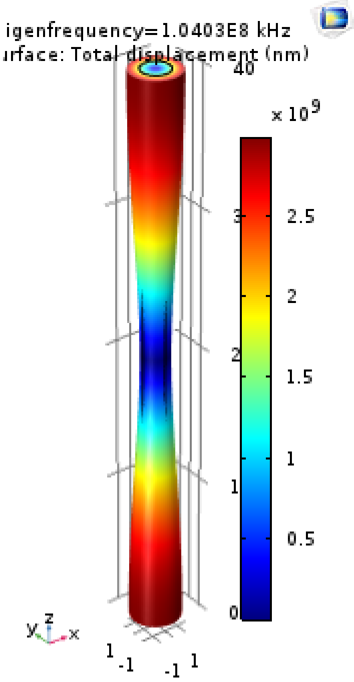

Mode 13

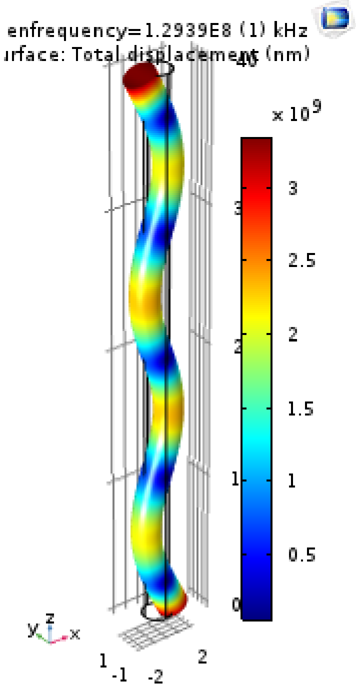

Mode 14

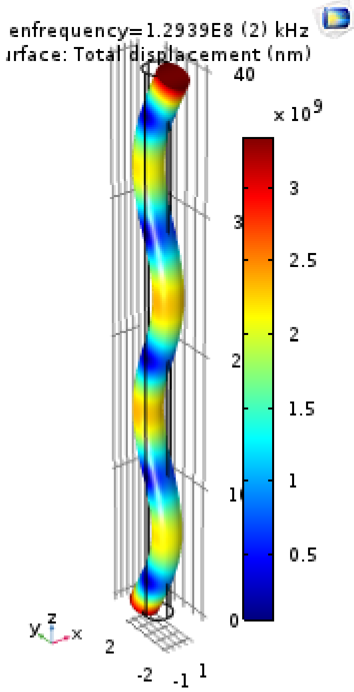

Mode 15

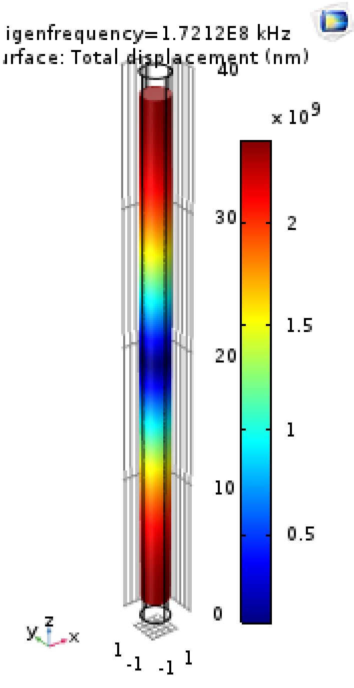

Mode 16

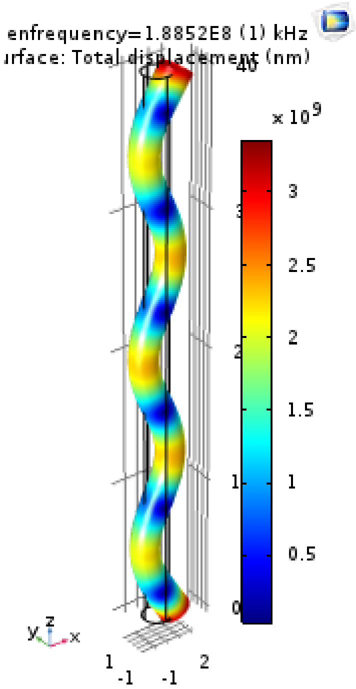

Mode 17

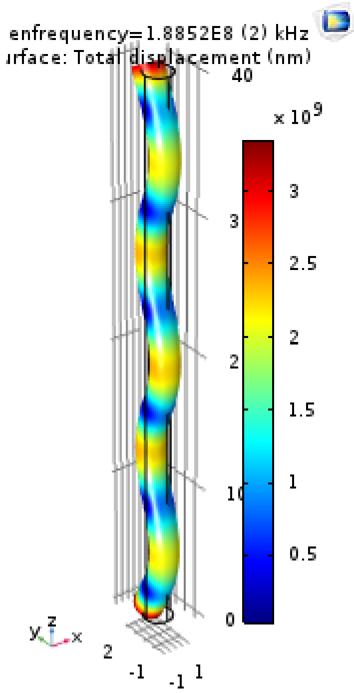

Mode 18

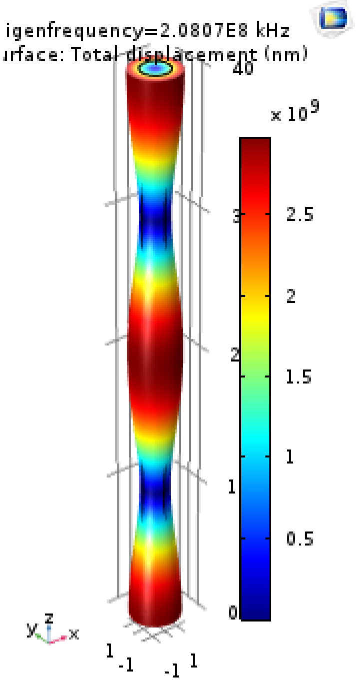

Mode 19

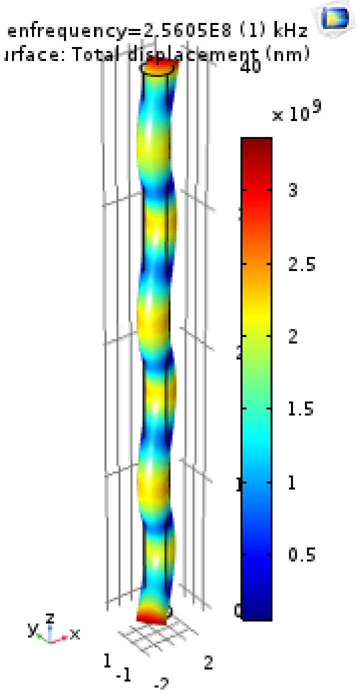

Mode 20

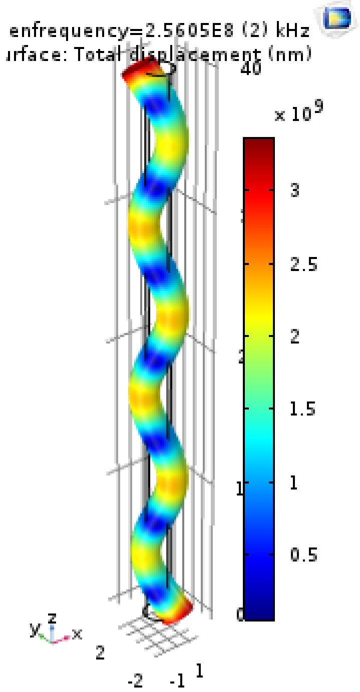

Mode 21

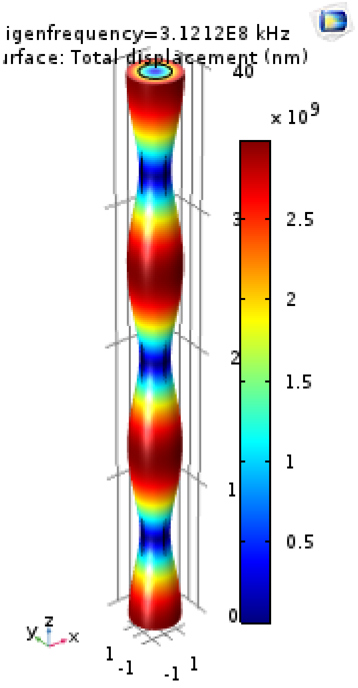

Mode 22

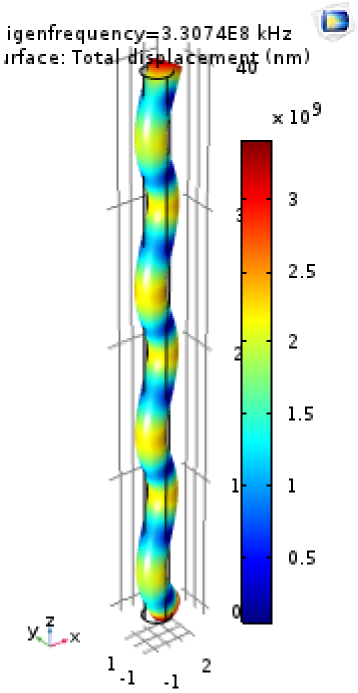

Mode 23

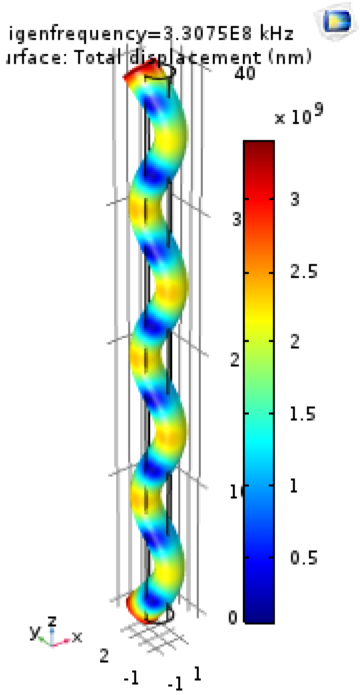

Mode 24

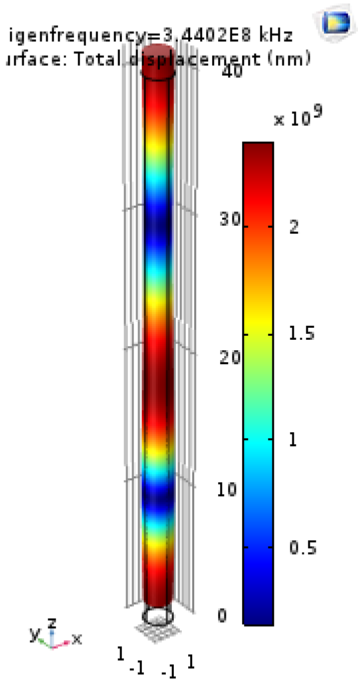

Mode 25

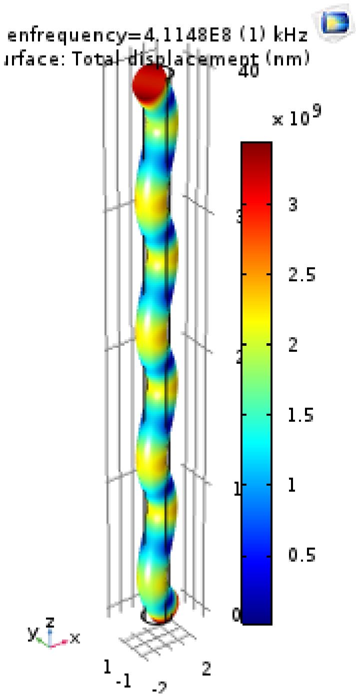

Mode 26

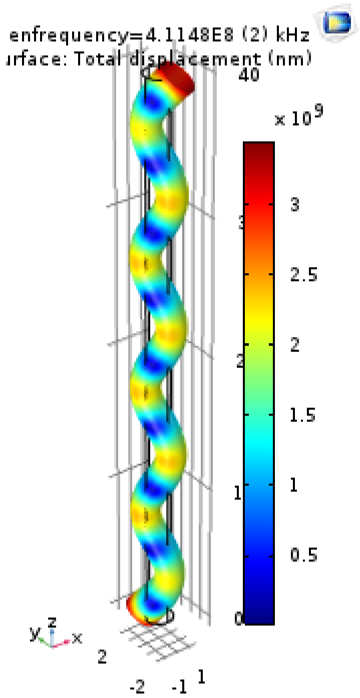

Mode 27

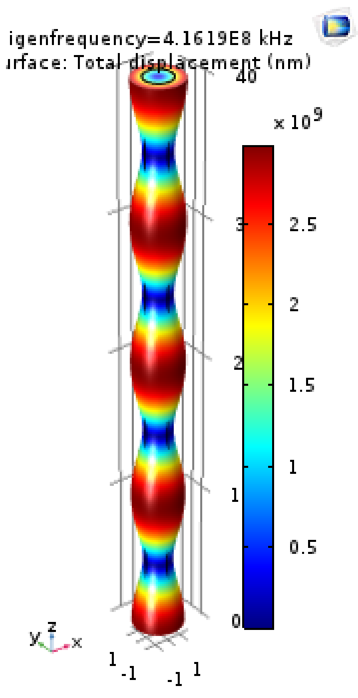

Mode 28

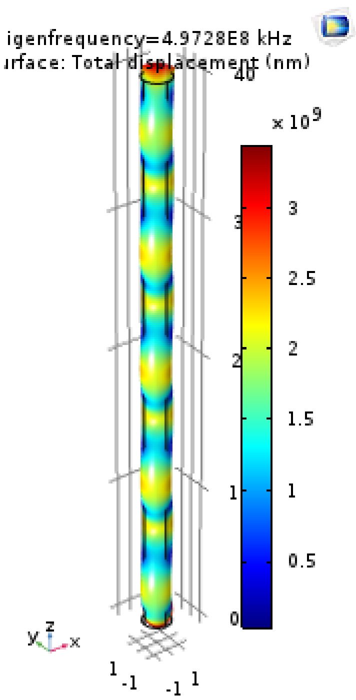

Mode 29

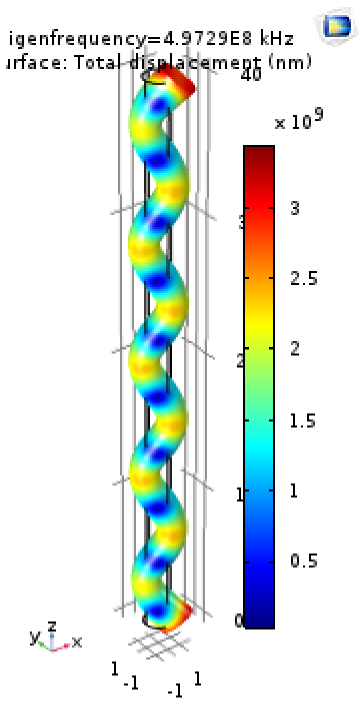

Mode 30

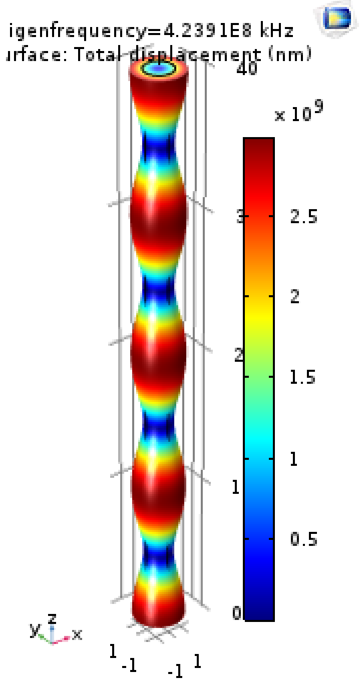

Mode 31

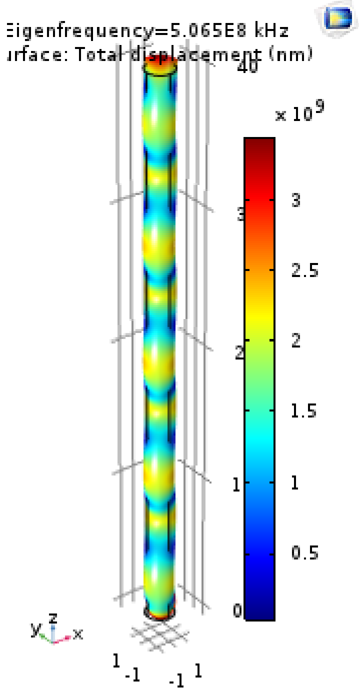

Mode 32

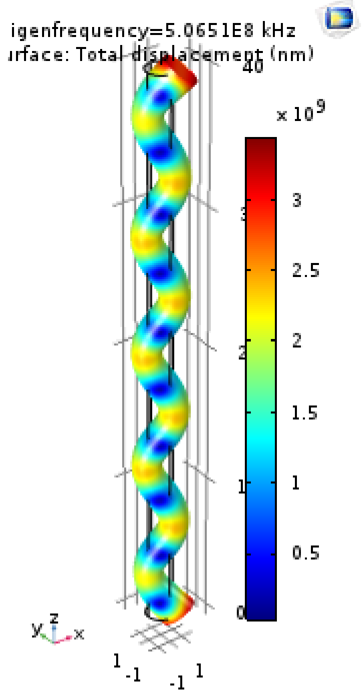

Mode 33

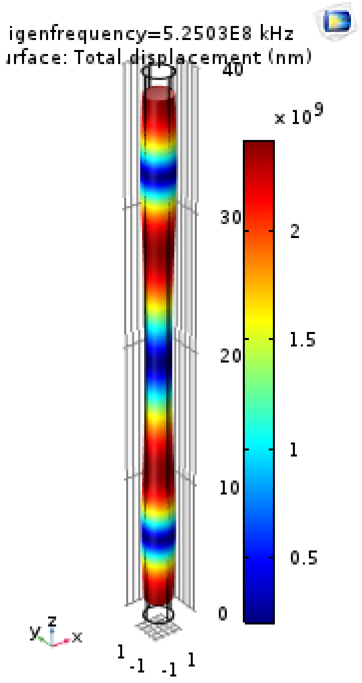

Mode 34

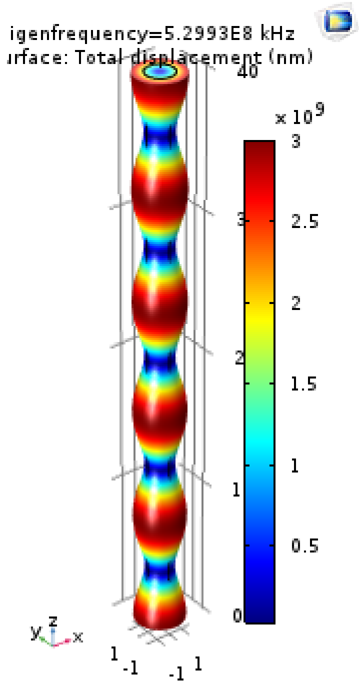

Mode 35

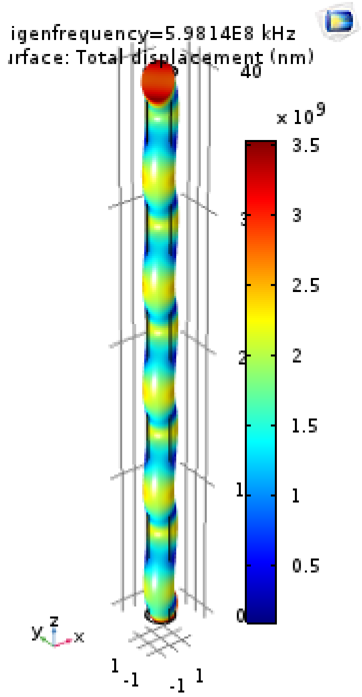

Mode 36

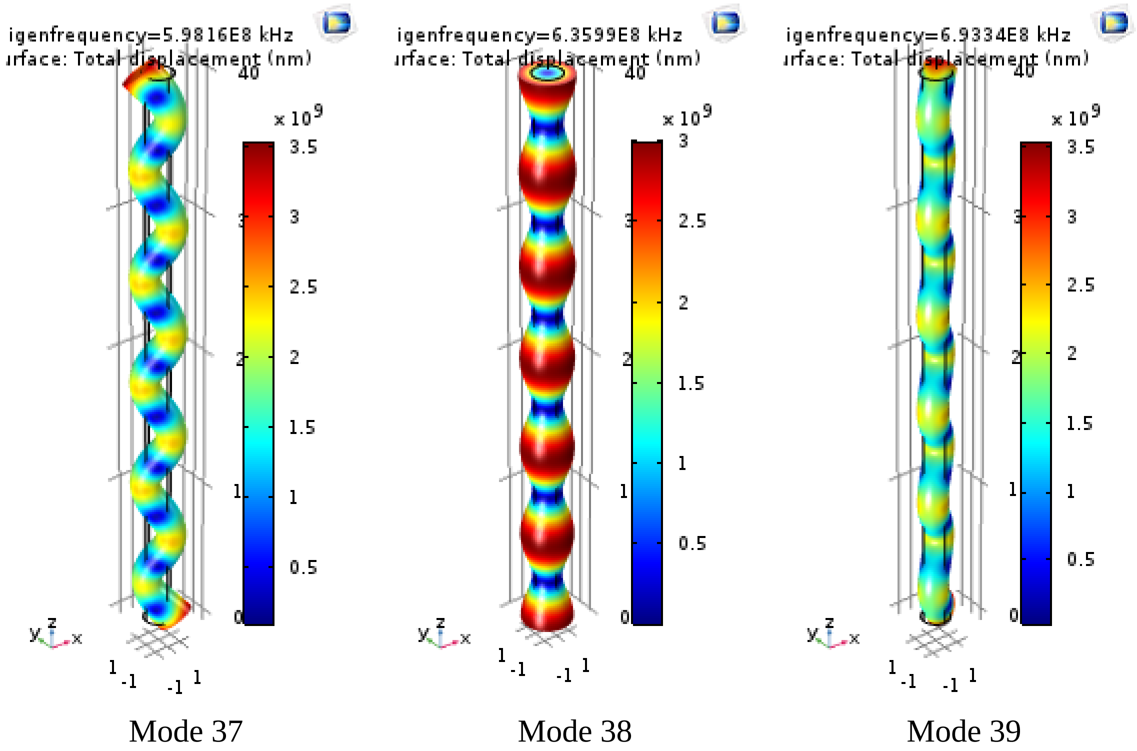

Fig. 2. First thirty-nine modes of SiCNW

The aim of the analysis is to obtain first ten eigenfrequency values and mode shapes of silicon carbide nanowire (SiCNW). First thirty-nine modes of SiCNW is calculated and results are demonstrated in Fig. 2. The cause to calculating thirty-nine modes is to obtain the proper first ten modal analysis results. As it can be clearly seen from Fig. 2, mode number calculated by the software include symmetrical modes and undesirable distensions modes. To overcome this issue, first ten mode numbers need to be selected carefully from thirty-nine mode shapes.

Sifting mode shapes can be easily done by visual choosing in current software. Familiar mode shapes can be easily differed from others while symmetric shapes need some more attention. In Fig. 3, selected and intended analyzes results is demonstrated with related eigenfrequencies.

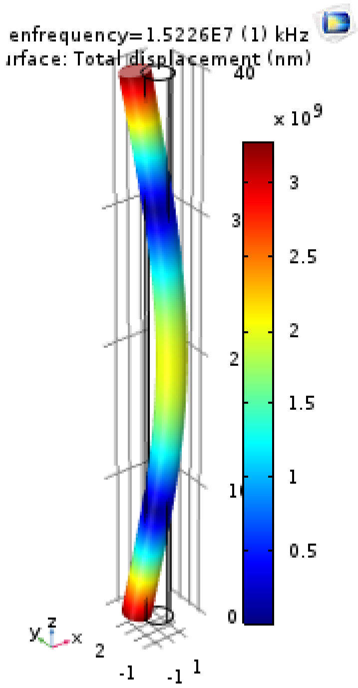

Mode 1

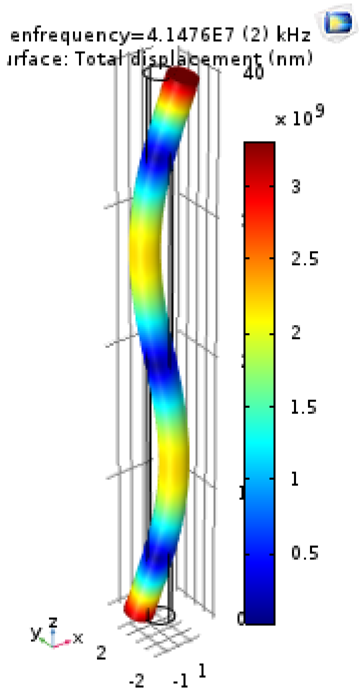

Mode 2

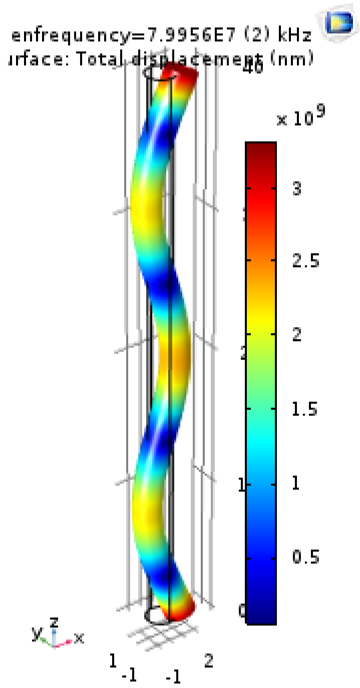

Mode 3

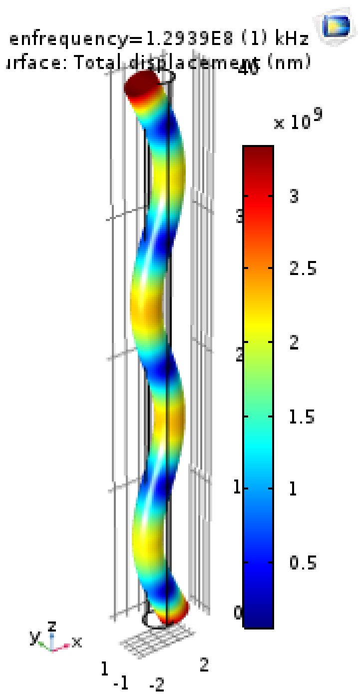

Mode 4

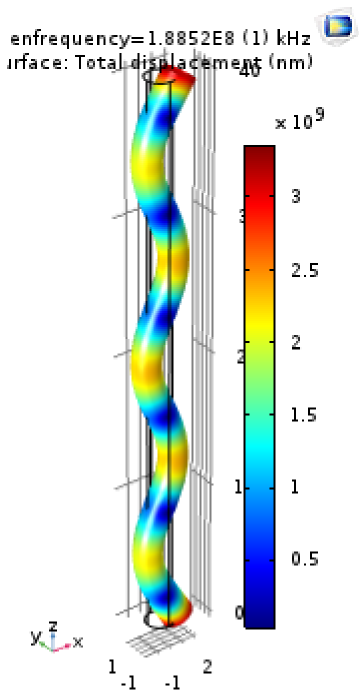

Mode 5

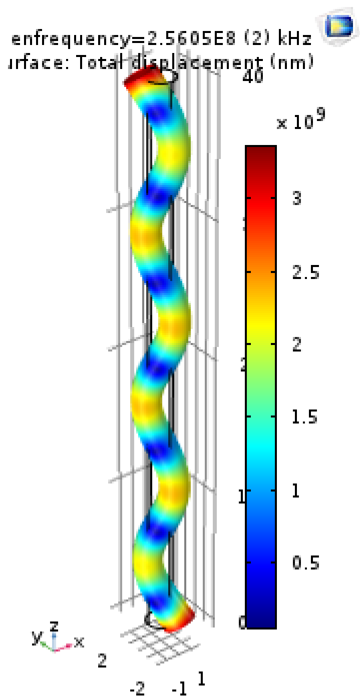

Mode 6

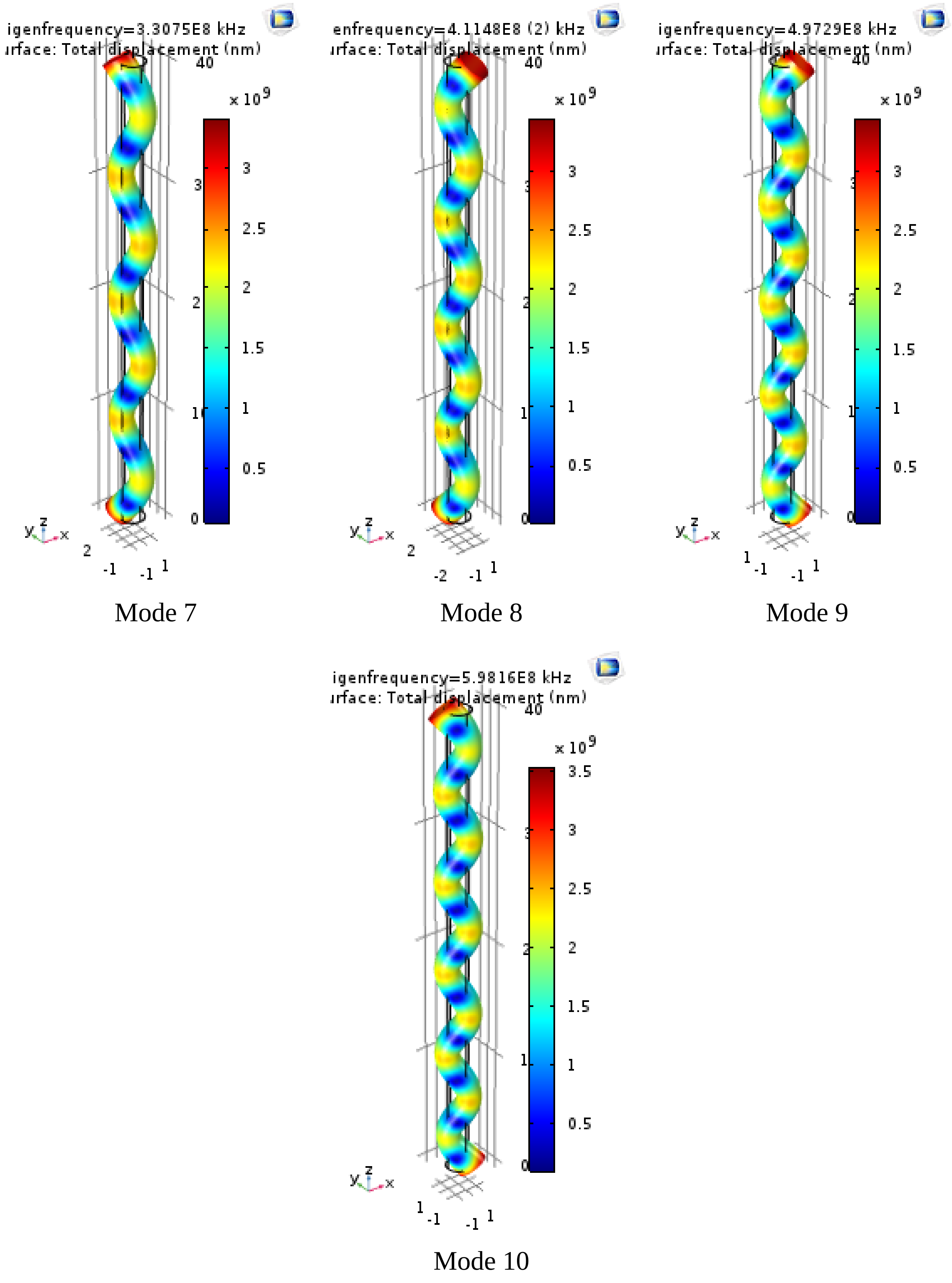

Fig. 3. Sifted first ten modes of SiCNW

5. Conclusions

In present study, the modal analysis of SiCNW is investigated using COMSOL Multiphysics computer software. Also, the right way of meshing and preparing micro and nano sized structures is demonstrated. To obtain intended first ten modes of SiCNW, thirty-nine modes needed to be calculated. After calculating mode shapes, results are sifted and desired first ten mode shapes are illustrated with related eigenfrequency value. This is a paper to give the introduction to finite element analysis softwares in micro and nano sizes. The future works can be comparing these results with size effective theories and see the validation of size effective constants.

Acknowledgements

The financial support of the scientific research projects unit of Akdeniz University is gratefully acknowledged.

References

[1] Civalek, Ö., Demir, C., Buckling and bending analyses of cantilever carbon nanotubes using the euler-bernoulli beam theory based on non-local continuum model. *Asian Journal of Civil Engineering*, 12(5), 651-661, 2011.

[2] Emsen, E., Mercan, K., Akgöz, B., Civalek, Ö., Modal analysis of tapered beam-column embedded in Winkler elastic foundation. *International Journal of Engineering & Applied Sciences*, 7(1), 1-11, 2015.

[3] Demir, Ç., Akgöz, B., Erdinç, M.C., Mercan, K., Civalek, Ö., Elastik bir ortamdaki grafen tabakanın titreşim hesabı. *Gazi Üniversitesi Mühendislik-Mimarlık Fakültesi Dergisi*, 32(2), 2017.

[4] Demir, C., Mercan, K., Numanoglu, H.M., Civalek, O., Bending response of nanobeams resting on elastic foundation. *Journal of Applied and Computational Mechanics*, 4(2), 105-114, 2018.

[5] Mercan, K., Civalek, Ö., Buckling analysis of silicon carbide nanotubes (SiCNTs). *International Journal of Engineering & Applied Sciences*, 8(2), 101-108, 2016.

[6] Avcar, M., Effects of rotary inertia shear deformation and non-homogeneity on frequencies of beam. *Structural Engineering and Mechanics*, 55(4), 871-884, 2015.

[7] Avcar, M., Effects of Material Non-Homogeneity and Two Parameter Elastic Foundation on Fundamental Frequency Parameters of Timoshenko Beams. *Acta Physica Polonica A*, 130(1), 375-378, 2016.

[8] Avcar, M., Mohammed, W.K.M., Free vibration of functionally graded beams resting on Winkler-Pasternak foundation. *Arabian Journal of Geosciences*, 11(10), 2018.

[9] Aktir, Y., Brunel, J.F., Dufrenoy, P., Mahe, H., Three-dimensional finite element model of an automotive clutch for analysis of axial vibrations. *Proceedings of the Institution of Mechanical Engineers Part D-Journal of Automobile Engineering*, 230(10), 1324-1337, 2016.

[10] Kim, B., Finite Element Modeling and Parametric Study of an Automotive V-belt Pulley for Durability Improvement. *International Journal of Precision Engineering and Manufacturing*, 16(7), 1517-1524, 2015.

[11] Kim, H.Y., Park, J.K., Lee, M.G., Phase transformation-based finite element modeling to predict strength and deformation of press-hardened tubular automotive part. *International Journal of Advanced Manufacturing Technology*, 70(9-12), 1787-1801, 2014.

[12] Le Henaff, F., Azzopardi, S., Woirgard, E., Youssef, T., Bontemps, S., Joguet, J., Lifetime Evaluation of Nanoscale Silver Sintered Power Modules for Automotive Application Based on Experiments and Finite-Element Modeling. *Ieee Transactions on Device and Materials Reliability*, 15(3), 326-334, 2015.

[13] Pisaturo, M., Senatore, A., Simulation of engagement control in automotive dry-clutch and temperature field analysis through finite element model. *Applied Thermal Engineering*, 93, 958-966, 2016.

[14] Toros, S., Altinel, K., Contribution of functionally graded material modelling on finite element simulation of rod end parts in automotive steering system. *Journal of Mechanical Science and Technology*, 30(7), 3137-3141, 2016.

[15] Wong, P.K., Xie, Z.C., Zhao, J., Xu, T., He, F., Analysis of automotive rolling lobe air spring under alternative factors with finite element model. *Journal of Mechanical Science and Technology*, 28(12), 5069-5081, 2014.

[16] Civalek, Ö., Geometrically non-linear static and dynamic analysis of plates and shells resting on elastic foundation by the method of polynomial differential quadrature (PDQ). 2004, Elazig: Firat University.

[17] Civalek, O., Finite Element analysis of plates and shells. 1998, Elazığ: Fırat University

[18] Civalek, O., Demir, C., A simple mathematical model of microtubules surrounded by an elastic matrix by nonlocal finite element method. *Applied Mathematics and Computation*, 289, 335-352, 2016.

[19] Jian, F.J., Jayas, D.S., Characterization of isotherms and thin-layer drying of red kidney beans, Part II: Three-dimensional finite element models to estimate transient mass and heat transfer coefficients and water diffusivity. *Drying Technology*, 36(14), 1707-1718, 2018.

[20] Mu, L.Z., Shao, H.W., He, Y., Oda, T., Jia, X.M., Construction of Anatomically Accurate Finite Element Models of the Human Hand and a Rat Kidney. *Journal of Mechanics in Medicine and Biology*, 11(5), 1141-1164, 2011.

[21] Snedeker, J.G., Bajka, M., Hug, J.M., Szekely, G., Niederer, P., The creation of a high-fidelity finite element model of the kidney for use in trauma research. *Journal of Visualization and Computer Animation*, 13(1), 53-64, 2002.

[22] Yates, K.M., Untaroiu, C.D., Finite element modeling of the human kidney for probabilistic occupant models: Statistical shape analysis and mesh morphing. *Journal of Biomechanics*, 74, 50-56, 2018.

[23] Das, A.K., Chatterjee, S., Finite element method-based modelling of flow rate and temperature distribution in an oil-filled disc-type winding transformer using COMSOL multiphysics. *Iet Electric Power Applications*, 11(4), 664-673, 2017.

[24] AB, w.c.c.C., COMSOL Multiphysics®. 2018: Stockholm, Sweden.

[25] Mercan, K., Civalek, O., Buckling analysis of Silicon carbide nanotubes (SiCNTs) with surface effect and nonlocal elasticity using the method of HDQ. *Composites Part B-Engineering*, 114, 35-45, 2017.

[26] Mercan, K., Numanoglu, H.M., Akgoz, B., Demir, C., Civalek, O., Higher-order continuum theories for buckling response of silicon carbide nanowires (SiCNWs) on elastic matrix. *Archive of Applied Mechanics*, 87(11), 1797-1814, 2017.

International Journal of Engineering & Applied Sciences (IJEAS)
Vol.10, Issue 4 (2018)305-309
http://dx.doi.org/10.24107/ijeas.504038
Int J Eng Appl Sci 10(4) (2018) 305-309

Identification Analysis of Control System Using Programming Language Python

Avtandil Bardavelidze [a] , Khatuna Bardavelidze [b] and Irakli Basheleishvili [c]*

[a,c]Akaki Tsereteli State University, Kutaisi, Georgia
[b] Georgian Technical University, Tbilisi, Georgia
E-mail address: basheleishvili.irakli@gmail.com

ORCID numbers of authors:
0000-0002-9873-4402 [a], 0000-0001-7972-47110 [b], 0000-0002-4429-7577 [c]

Received date: 27.12.2018
Accepted date: 10.01.2019

Abstract

The paper describes the matrix parameters of continuous control system by a regression approach: state -space equation in the continuous or discrete forms. The example of the system regression analysis is discussed according to the example of residual moisture stabilization system of material in a drying apparatus, the structural scheme is given. The coefficients of state space equation are represented by matrix and numeric value. The obtained results are graphically illustrated. The modern and widespread programming language Python and Python Control System Library are used at all stages of research.

Keywords: Control system, identification, regression analysis, verification, state-space.

1. Introduction

Today, the methods of Regression Analysis have been successfully used to process the experimental data in Biology, Economics, Automation and other fields. In regression analysis all available resources should be used completely and efficiently, especially if we are dealing with the accumulation and processing of information. The development and perfection of the identification method are required for increasing the accuracy and reliability of dynamic objects in many fields of science and technology. Today, the most required methods of evaluation of experimental data provide high rates of efficiency, reliability, consumed energy savings and memory volume. Solving the problems of processing numerical algorithm for signals and parameters evaluation in linear dynamic object will solve all practical tasks. The purpose of the work is to evaluate the matrix parameters of control system with regression approach by using the programming language Python and integrated Python Control Systems Library

2. Theoretical Part

The state-space equation of continuous system has the form [1]:

$$\begin{cases} \dot{X}(t) = AX(t) + BU(t) \\ Y(t) = CX(t) + DU(t) \end{cases} \quad (1)$$

Where X(t) - is a state vector n size; U(t) - is a control vector size r ; Y(t) - is a system output vector size; A - n×n state matrix size; BC and D=0 input, output and zero (null) matrix. In our case the task is to determine the matrix real numbers _ A, B, C, D of system parameters. (1) should be represented by the discrete forms for regression analysis of the system:

$$\begin{cases} X[(k+1)T] = A_d X(kT) + B_d U(kT) \\ Y(kT) = CX(kT) + DU(kT) \end{cases} \quad (2)$$

Where T – is a by quantization step by time; K- whole number; C,D –is a matrix discrete system of the same dimension, that is the initial continuous system.

A_d and B_d matrices have the following form[2]:

$$A_d = e^{AT}, \quad (3)$$

$$B_d = \int_0^T e^{AT} BT. \quad (4)$$

3.Practical Part

We should only use input impact and the value of state vector to evaluate the matrix parameters. Let's consider A and B matrix regression analysis of control system for the open system of the residual moisture stabilization of material in a drying apparatus, that consists of three inertial parts with the following parameters: $K_1 = 0{,}2$, $T_1 = 16$ s; $K_2 = 0{,}2$, $T_2 = 6{,}6$ s; $K_3 = 0{,}15$, $T_3 = 2$s[3]. Obtain the input impact on the system in the form of $u(t) = e^{-0{,}6t}\cos(2t)$. Obtain the system initial condition as a zero in the state variable The open system of the residual moisture stabilization of the drying material in the drill drying apparatus has the following form:

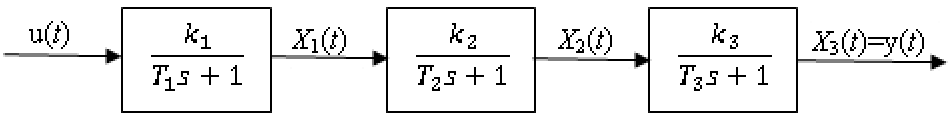

Fig. 1. Open System of residual moisture stabilization

The transfer function of the system is determined for zero initial conditions; therefore, s complex variable may be formally changed by the product. So finally, the connection between the input and output values of the system may be represented by the following differential equation:

$$\dot{x}_1(t) = -\frac{1}{T_1} x_1(t) + \frac{k_1}{T_1} u(t);$$

$$\dot{x}_2(t) = \frac{k_2}{T_1} x_1(t) - \frac{1}{T_2} x_2(t); \quad (5)$$

$$\dot{x}_3(t) = \frac{k_3}{T_3}x_2(t) - \frac{1}{T_3}x_3(t).$$

System may be represented by a matrix form and the matrix of control system will have the following form:

$$A = \begin{bmatrix} -\frac{1}{T_1} & 0 & 0 \\ \frac{k_2}{T_2} & -\frac{1}{T_2} & 0 \\ 0 & \frac{k_3}{T_3} & -\frac{1}{T_3} \end{bmatrix}, B = \begin{bmatrix} \frac{k_1}{T_1} \\ 0 \\ 0 \end{bmatrix}, C = [0, \quad 0, \quad 1], D = 0, \quad (6)$$

Taking into account the numeric values of the parameters of the system inertial parts, we will obtain: The transformation of discrete system into matrix continuous system is implemented by specialized functions: ss(Create a state space system), d2c(discrete to continuous conversion), ssdata(Return state space data objects for a system)[4].
The results of the program implementation have the following form:

```
A =
     -0.0625         0            0
      0.0303    -0.1515         0
       0            0.0750   -0.5000

B =
     0.0125
       0
       0

C =
      0     0     1

D =
      0

Ad =
      0.9994        0             0
      0.0003    0.9985         0
      0.0000    0.0007    0.9950

Bd =
   1.0e-003 *
       0.1250
      -0.0000
       0.0000
Adr =
   0.9994   -0.0000    0.0000
   0.0003    0.9985    0.0000
   0.0000    0.0007    0.9950

Bdr =
  1.0e-003 *
   0.1250
       -0.0000
```

0.0000
Areg =
-0.0625 -0.0000 0.0000
0.0303 -0.1515 0.0000
0.0000 0.0750 -0.5000
Breg =
0.0125
-0.0000
0.0000

Whose transition characteristics are shown in Fig.2. The analysis of the obtained results shows that the evaluation of the matrix system is quite accurate.

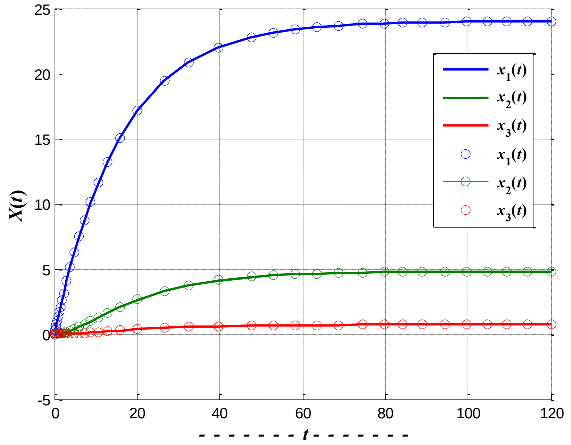

Fig. 2. Transfer functions of state variables

On the other hand, let's do the regression evaluation of the matrix output parameters of the same system. Matrices of control systems are determined by (6) the images. We have made the regression identification of C output matrix based on the equation $Y(t) = CX(t)$. The results of the program implementation are represented by the following way:

C =
0 0 1
Cdr =
0.0000 0.0007 0.9950
Creg =
0.0000 0.0007 0.9950

The diagram of the system output process in verification is shown in Fig. (3).

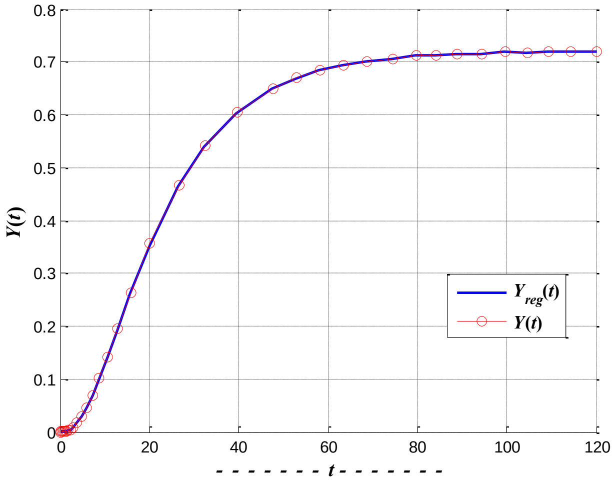

Fig. 3. Transition process on the system output

4. Conclusions

As a result of the survey, the regression evaluation of the matrix of continuous linear system is sufficiently accurate. Such approach of the system regression analysis may be successfully used in various fields that will give us the ability to use all available resources in full and efficient manner.

References

[1] Дроздов А.Л. Алгоритм идентификации характеристик динамической системы по данным наблюдений. Автоматика и телемеханика, 58-66, 2000.

[2] Bardavelidze, A., Basheleishvili, I., Bardavelidze, K. Research Investigation on Automatic Control System of Drying Apparatus Based on Fuzzy Logic. Journal of Technical Science and Technologies, 6(1), 2017.

[3] Bardavelidze, A., Basheleishvili, I., Bardavelidze, K. Predication Digital Control System For A Drying Apparatus. Computer Science & Telecommunications, 54(2), 2018.

[4] Bardavelidze, K Optimal Digital Control System of Drying Apparatus. Journal of Technical Science and Technologies, 2(1), 33-35, 2014.

[5] Bucher, R. Python for control purposes. (2018).